Interior Exploration Using Seismic Investigations, Geodesy, and Heat Transport (InSight) Mission

Insight Fluxgate Magnetometer (IFG)

InSight IFG Data Calibration Description

Prepared by

Steven Joy (in-flight calibration lead)

Katheryn Rowe (ground calibration lead)

Version 2.0

September 28, 2023

Contents

1 Introduction

1.1 Document Change Log

Table 1: Document change log.

Version	Change	Date	Affected portion
1.0	Initial draft	April 29, 2019	All
1.1	Updated to describe the new data processing method (v07)	June 21, 2023	
1.2	Updated to include peer review comments	September 21, 2023	

1.2 Purpose

This document provides the details of the IFG data calibration process and examples of the various types of issues that have been identified in the raw data, and the data after the ground calibration has been applied. This document provides much more detail than the IFG Archive SIS, although some of the contents of the SIS are repeated here. The purpose of the SIS is to provide a description an overview of the dataset, the data processing, and the structure of the archive. This document focuses exclusively on the calibration process and processing. For details about the archive organization, contents, naming conventions, etc. the reader is referred to the IFG archive SIS.

IFG data are processed by first applying the ground calibration which results converts the raw data numbers to nanoTesla and orthogonalizes the sensor data giving data in the instrument frame. The resulting data show large diurnal variations that are well correlated with the instrument temperatures and the solar array currents. The in-flight calibration first removes the component of the diurnal variation that is correlated with these spacecraft sources. Once the low frequency corrections have been applied, the procedure is to identify high frequency variations and remove them when possible.

1.3 References

[1] Chi, P., Russell, C., Yu, Y., Joy, S., Ma, Y., Banfield, D., et al. (2019). InSight observations of magnetic pulsations on Martian surface: Morphology and wave sources. AGU fall meeting abstracts, (pp. DI51B–0024).

[2] Johnson, C. L., Mittelholz, A., Langlais, B., Russell, C. T., Ansan, V., Banfield, D., et al. (2020). Crustal and time-varying magnetic fields at the InSight landing site on Mars. Nature Geoscience, 13(3), 199–204. https://doi.org/10.1038/s41561-020-0537-x

[3] A. Mittelholz, C. L. Johnson, M. Fillingim, R. E. Grimm, S. Joy, S. N. Thorne, W. B. Banerdt (2023), Mars' External Magnetic Field as Seen From the Surface With InSight, J. Geophys Res.: Planets, 128:1, https://doi.org/10.1029/2022JE007616.

[4] Thorne, S. N., Mittelholz, A., Johnson, C. L., Joy, S., Liu, X., Russell, C. T., et al. (2020)., InSight fluxgate magnetometer data calibration assessment and implications., 51st Lunar and Planetary Science Conference, LPI Contribution No. 2326, id.1331, bibcode: 2020LPI....51.1331T

1.4 Abbreviations

Table 2: List of abbreviations

Abbreviation	Meaning
AOBT	APSS Onboard Time
APSS	Auxiliary Payload Sensor Suite
ASCII	American Standard Code for Information Interchange
dB_i	Delta B, i^{th} component (nT)
dB_Cur	Computed dB computed from solar array current response (SA and SACT)
dB_Temp	Computed dB computed from temperature response (Sensor and Electronics)
COMM	Communications (RISE-COMM or Lander-COMM)
DC	Zero frequency
DN	Data Number
DQF	Data quality flag
ET	Electronics temperature (^oC)
FSAC, SA	Fixed solar array current
FEI	File Exchange Interface
FIR	Finite Impulse Response (filter)
FM	Flight module
FSW	Flight Software
GB	Gigabyte(s)
GC	Ground calibration
HK	Housekeeping data
Hz	Hertz
ICD	Interface Control Document
IFG	Insight Fluxgate Magnetometer
IGPP	Institute of Geophysics and Planetary Physics
IOC	IFG Operation Center
IM	Information Model
ISO	International Standards Organization
JPL	Jet Propulsion Laboratory (Pasadena, CA)
LA	Lander activity

Abbreviation	Meaning
LID	Logical Identifier
LIDVID	Versioned Logical Identifier
MAVEN	Mars Atmosphere and Volatile EvolutioN spacecraft
MLST	Mean Local Solar Time
model*, modSACT	Model Sensor Temperature (ST), Model Electronics Temperature (ET), model fixed Solar Array current (SA), model total solar array current (SACT)
NAIF	Navigation and Ancillary Information Facility (JPL)
nT	Nanotesla
PAE	Payload Ancillary Electronics
PDS	Planetary Data System
PDS4	Planetary Data System Version 4
RISE	Rotation and Interior Structure Experiment
SC. S/C	Spacecraft
SCLK	Spacecraft Clock
SECA	Spacecraft engineering and ancillary (data)
SEIS	Seismic Experiment for Investigating the Subsurface
SIS	Software Interface Specification
SP	Short Period
ST	Sensor temperature (°C)
TBD	To Be Determined
TLST	True Local Solar Time
TSAC, SACT	Total solar array current
UCLA	University of California, Los Angeles
URN	Uniform Resource Name
UTC	Universal Time Coordinated
XML	eXtensible Markup Language

2 Ground Calibration

Prior to delivery to the project for spacecraft integration, the InSight Fluxgate Magnetometer (IFG) instrument response was characterized over a range of temperatures similar to the expected Martian environment that could be achieved in the laboratory setting. The following tables and charts summarize the results of those efforts.

Table 3: Scale Factors.

Data Type	Scaling	Units
X-Axis	Divide by 145.6	nT
Y-Axis	Divide by 141.4	nT
Z-Axis	Divide by 141.7	nT
HK0 (+8V)	Divide by -181.23, add 20.91	V
HK1 (AGND)	Divide by -64, add 38.31	V
HK2 (SH Temp)	$9E\text{-}05x^2\text{-}0.576x+803.43$	ºC
HK3 (EU Temp)	Divide by -7.3, add 333.5	ºC
HK4 (+13V)	Divide by -219.3, add 21.8	V

Scale factors are used to convert engineering data number to physical units.

Table 4: IFG Performance (24 bit digitization).

Dynamic Range of X-Axis	±20,600nT
Dynamic Range of Y-Axis	±21,200nT
Dynamic Range of Z-Axis	±21,200nT
Offset of X-Axis @ 24°C	-71.6nT
Offset of Y-Axis@ 24°C	-57.3nT
Offset of Z-Axis @ 24°C	-0.5nT
Data Rate of X, Y, Z	20 samples per second
Bandwidth of X-Axis	3dB @ 9Hz
Bandwidth of Y-Axis	3dB @ 9Hz
Bandwidth of Z-Axis	3dB @ 9Hz
Noise levels of X, Y, Z	Less than 30pT/√Hz @ 1Hz

Figure 1: Noise Levels below 0.3 nT (shown in yellow).

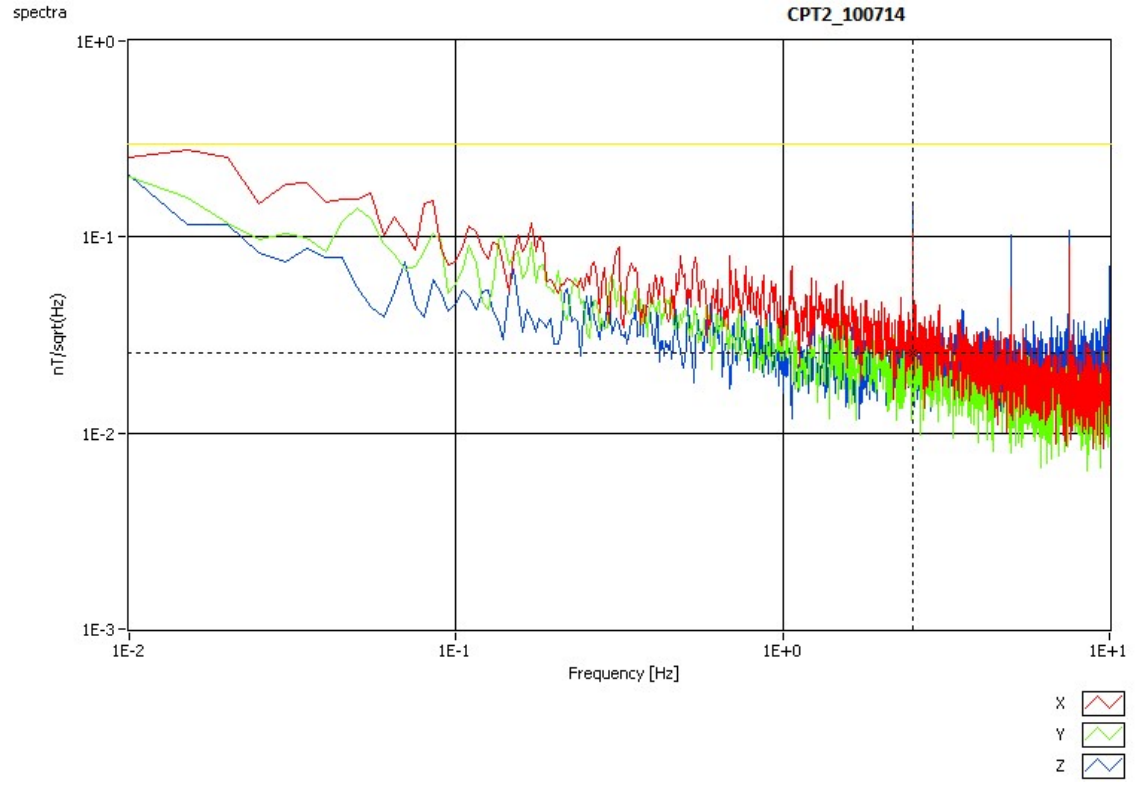

Figure 2: Sensor stability over 24 hours.

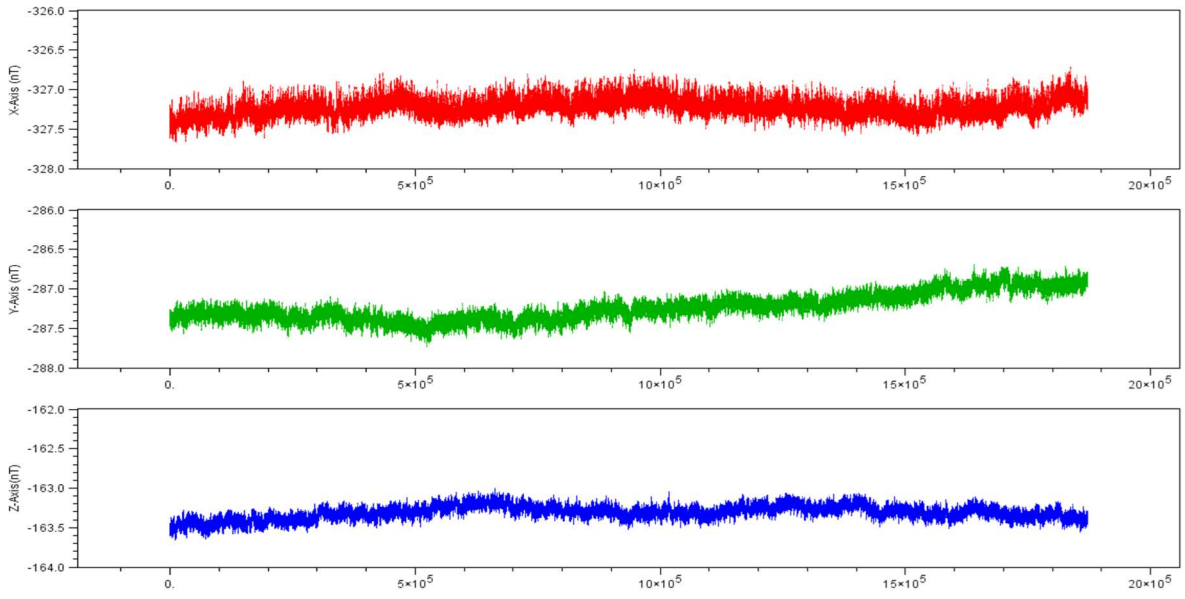

Transfer function: The digital filter used in the IFG is a 400 point boxcar filter, with a gain of $400/2^9$.(Also can be represented as a coefficient of 1/512, with 400 points). The digital filter dominates the end-to-end transfer function.

Figure 3: Transfer Function (between DC-10 Hz).

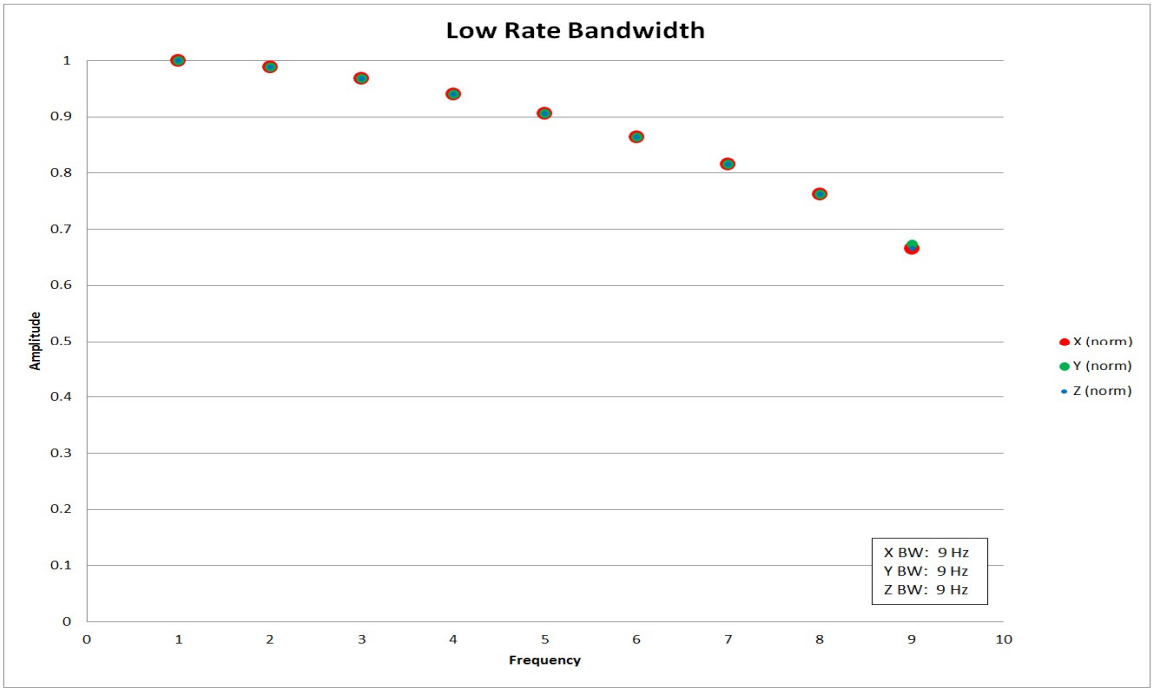

Figure 4: Transfer function (between DC-120Hz).

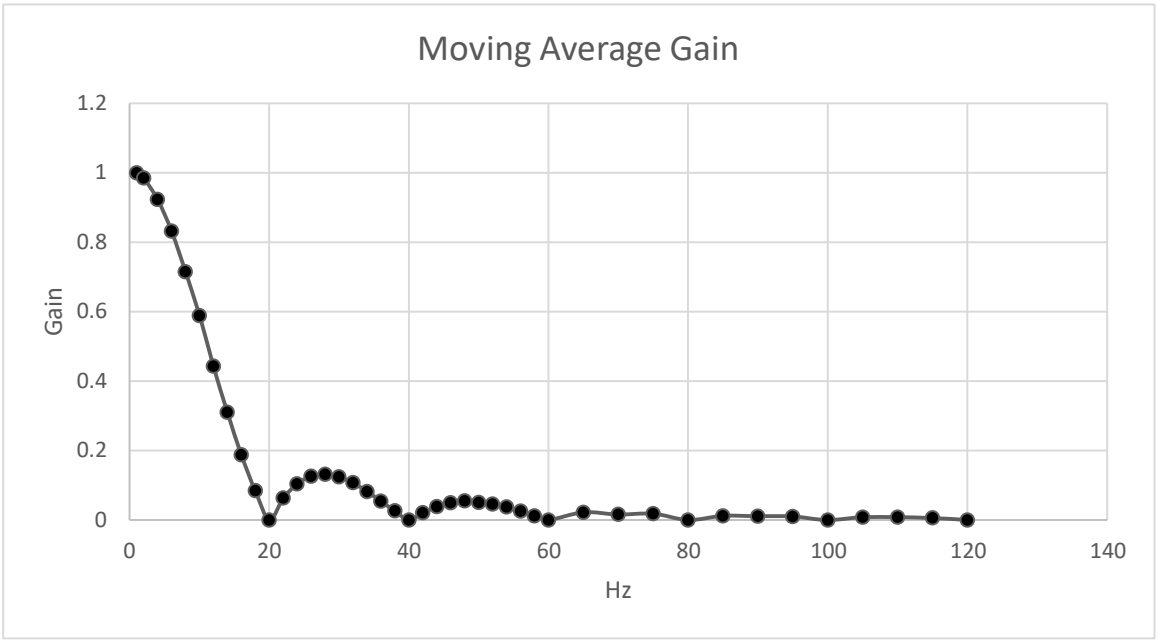

Figure 5: Electronics thermal stability - Offset temperature dependence.

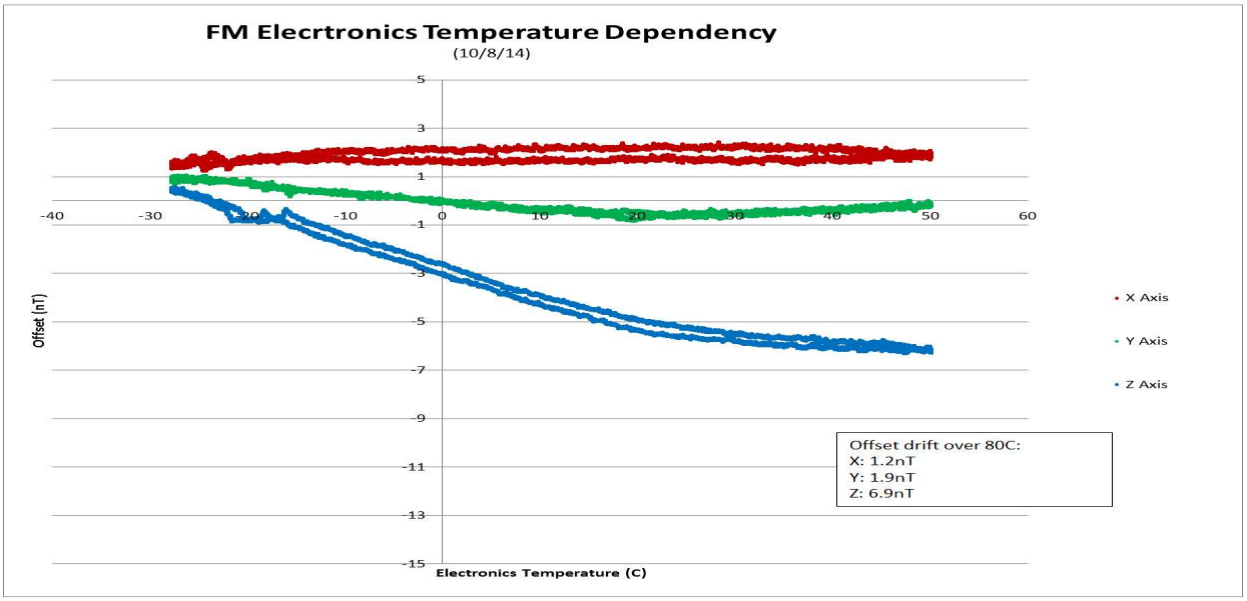

Figure 6: Electronics thermal stability - Gain temperature dependence.

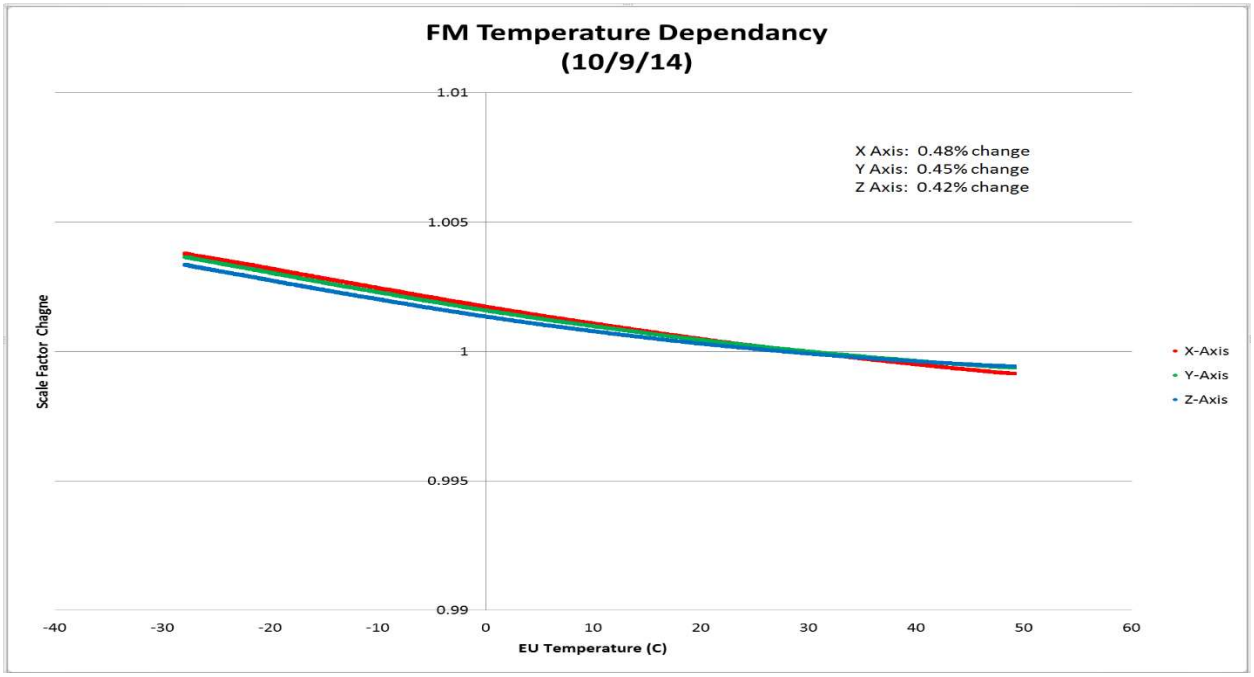

Offset X: $y = -0.0002x^2 + 0.0073x + 1.8809$ Offset Y: $y = 0.0005x^2 - 0.0275x - 0.1188$ Offset Z: $y = 0.0009x^2 - 0.1085x - 3.0463$	Gain X: $y = 3E\text{-}07x^2 - 7E\text{-}05x + 1.0017$ Gain Y: $y = 4E\text{-}07x^2 - 6E\text{-}05x + 1.0016$ Gain Z: $y = 4E\text{-}07x^2 - 6E\text{-}05x + 1.0013$

Note that a 0.5% change in a 1,000 nT field is 5 nT over the 80 ^{o}C change in temperature.

Figure 7: Sensor head thermal stability - Offset temperature dependence.

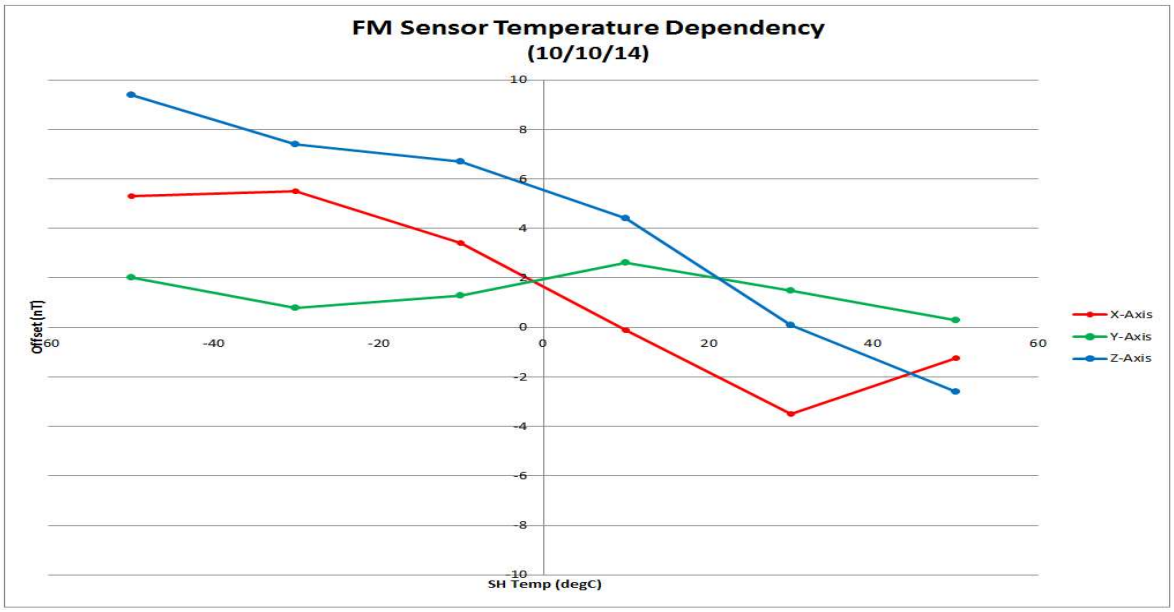

Offset X: $y = 0.0002x^2 - 0.0904x + 1.2953$ Offset Y: $y = -0.0003x^2 - 0.0073x + 1.75$ Offset Z: $y = -0.0008x^2 - 0.1203x + 5.1656$	Gain X: $y = 1E\text{-}06x^2 + 0.0004x + 0.9916$ Gain Y: $y = 7E\text{-}07x^2 + 0.0003x + 0.991$ Gain Z: $y = 8E\text{-}07x^2 + 0.0002x + 0.9948$

Figure 8: Sensor head thermal stability - Gain temperature dependence.

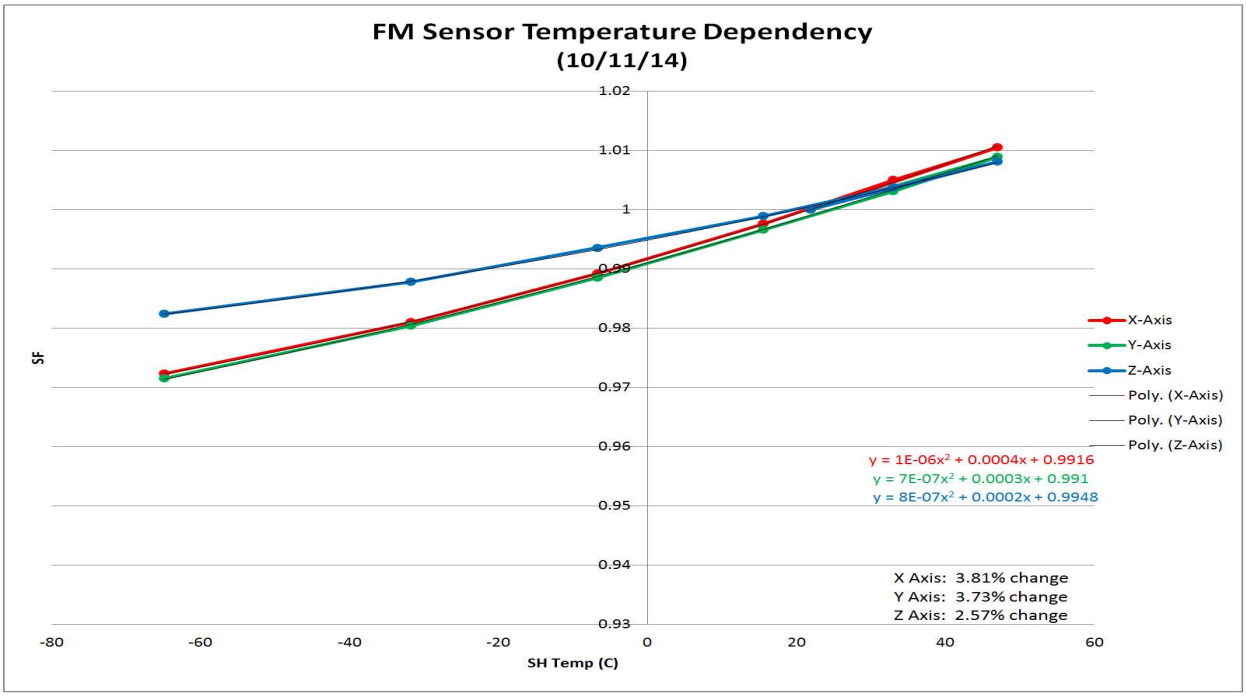

Note that a 3.8% change in a 1,000 nT field is 38 nT over the 120 ºC change in temperature, and that the ground calibration did not extend below -70 ºC.

3 In-flight Calibration

Initially, the InSight IFG were processed just using the ground calibration values. However, the resulting field values showed an unexpectedly large diurnal variation when only processed to this level. Figure 9 shows a few SOLs of data shortly after landing with just the ground calibration applied. The three IFG data panels (bottom 3) show the data on a 200 nT vertical scale.

Figure 9: Early landed IFG data with ground calibration applied.

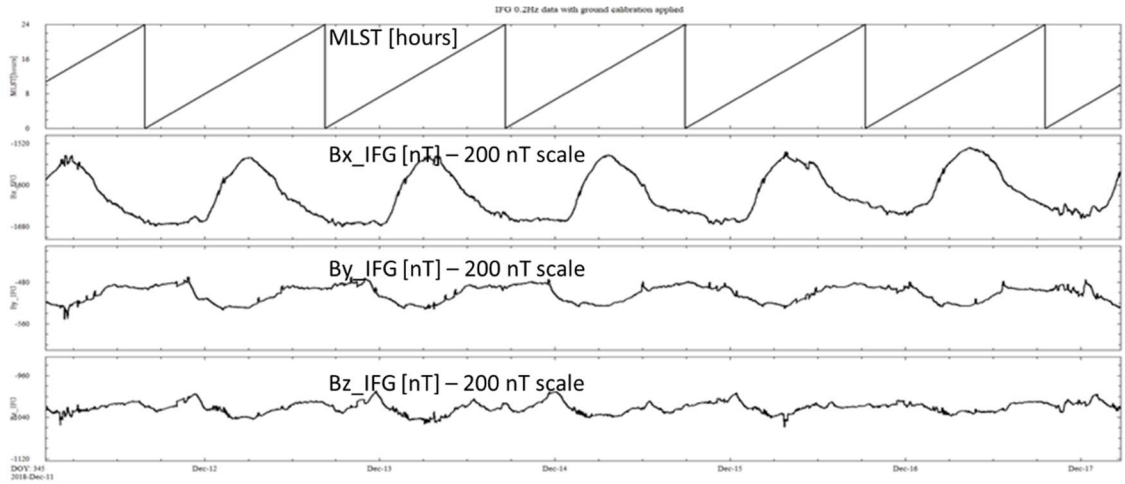

The IFG team initially showed that there was a strong correlation between the temperatures and the observations and the data were initially decorrelated with the temperature data. However, the resulting data still showed larger than expected diurnal variations. After some further investigation, the data were shown to also be correlated with the solar array current data. Figure 10 shows the diurnal variation in the IFG temperatures and solar array currents and Figure 11 shows the

Figure 10: Diurnal variation in IFG temperatures and solar array currents.

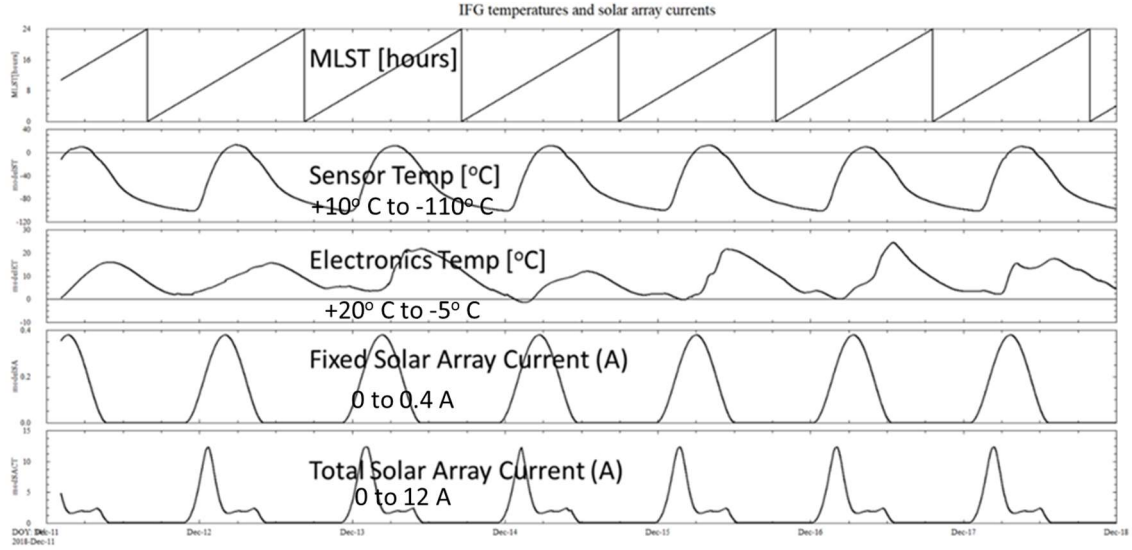

coherence (left) and phase (right) between the sensor (top) and electronics (bottom) temperatures and the fixed solar array currents (middle). Note that while the sensor temperature and solar array currents are in phase with the IFG data, the electronics temperature is out of phase. Additional analysis showed that there was an additional correlation with the total solar array current as well.

Figure 11: IFG Coherence with temperature and fixed solar array currents.

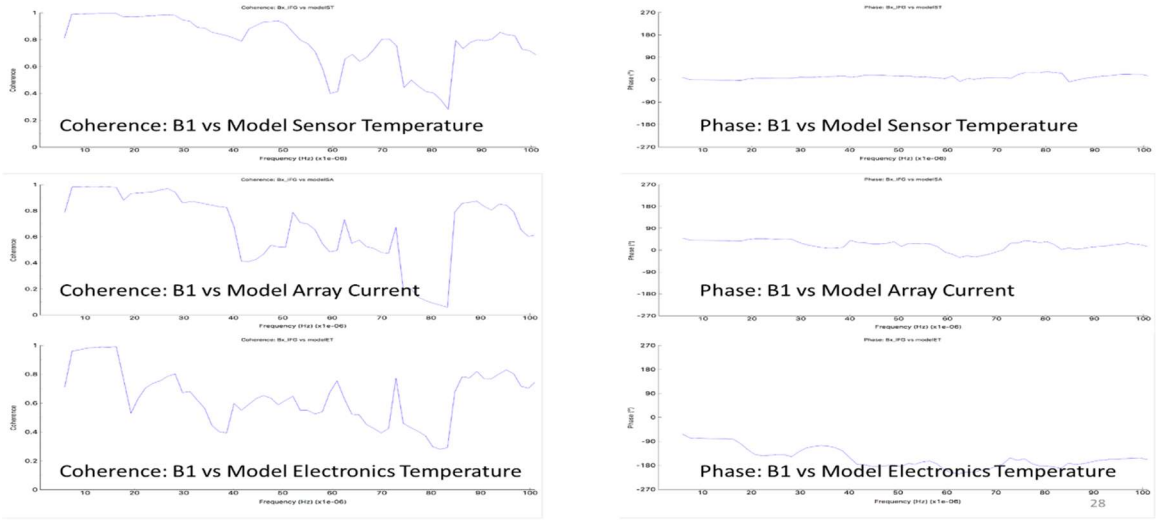

3.1 Initial Data Processing (v01 - v06)

The IFG data are decorrelated with the temperature and current data by assuming that the diurnal variation associated with these parameters can be represented as a linear function of the four variables, and the subtracting the resulting function from the data. The daily perturbation is calculated as the difference between the observed field and the mean value observed at 20:00 TLST. The local time was selected because the solar array currents have gone to zero and the temperatures (sensor temp ~ -60 ^{o}C, elect temp ~20 ^{o}C) are within the range that was calibrated in the laboratory (see Figures 5-8). The mean value of the field that is used for this calculation is (-1645, -500, -1045) nT in the IFG frame. These values are subtracted from the data and then the residuals (dB_i) are fit as a linear function of the temperatures and solar array currents of the form:

$$(1)\quad dB_i = C_{0,i} + C_{1,i} * ST + C_{2,i} * ET + C_{3,i} * FSAC + C_{4,i} * TSAC$$

where the C are the constants determined by the fit, ST and ET are the sensor and electronics temperatures (modelSA and modelET) in ^{o}C respectively, and FSAC and TSAC are the fixed and total solar array (modelSA and modSACT) currents in Amps respectively. During the spacecraft commissioning, the spacecraft environment was changing frequently. We found that a given set of coefficients could be used for only a few days to weeks. The fit coefficients and time range of applicability is provided with the archive in the file called PolynomialFits.txt (LID: urn:nasa:pds:insight-ifg-mars:document:polynomial-fits) in the document collection of the insight-ifg-mars bundle. We were hopeful that the frequency at which new fits and models of the current systems used in the fitting process will decrease once commissioning is complete. In theory, after that time there should only be seasonal changes and those attributable to dust on the solar arrays.

Figure 12 shows the same time interval as Figures 9 and 10, and the same vertical scales, after the calculated dBi's have been subtracted from the data. Figure 13 shows the same time interval on a 75 nT scale. After correction, a diurnal variation in the field that is on the order of 35 nT remains. Of this residual, some portion is likely to be associated with one or more current systems on the spacecraft that have not yet been identified. The IFG team has looked at the various current data

Figure 12: IFG data after decorrelation applied.

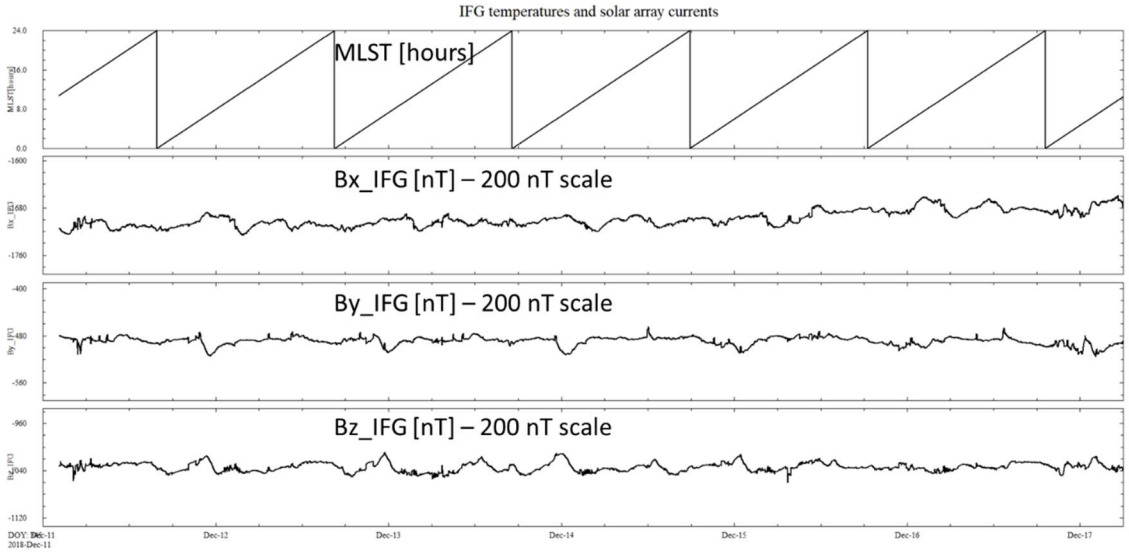

that are included in the spacecraft engineering and ancillary data provided and have not identified any channels that are well correlated with the residual diurnal signal in the IFG data. This lack of correlation leads us to believe that most of the residual variation in the data are not the result of spacecraft sources.

Figure 13: IFG data after decorrelation on a 75 nT scale.

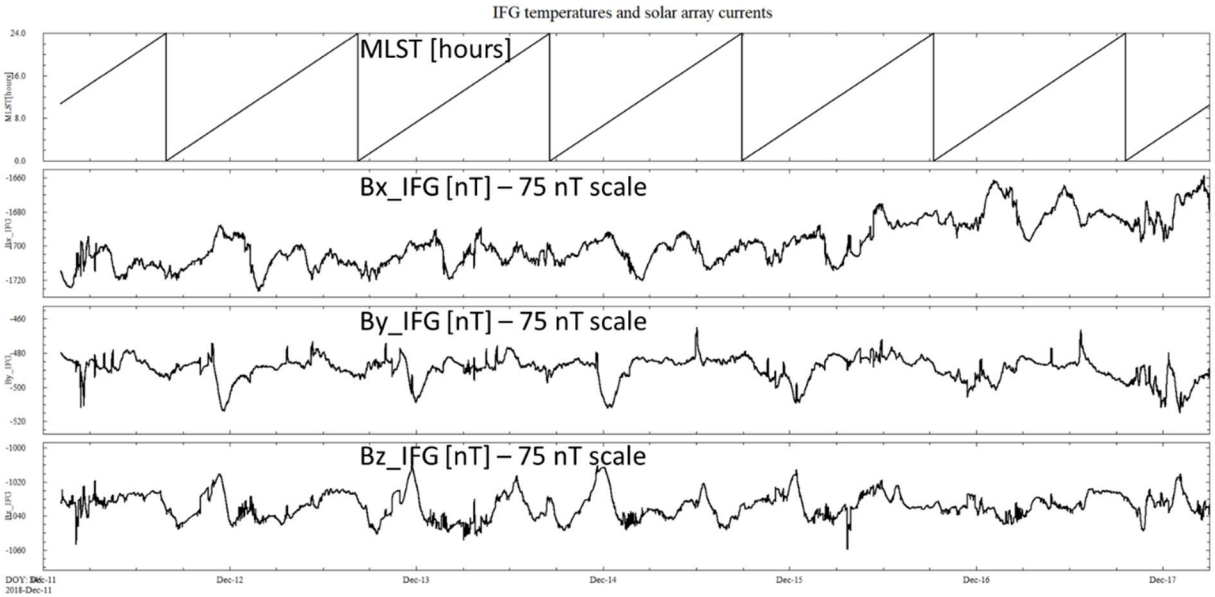

The computation of the delta **B** associated with these thermal and current variations requires a continuous measure of those parameters which is not provided in the InSight spacecraft engineering and ancillary data. Models of the TLST variations in these parameters have been developed to provide the continuous input required. The appendices of this document describe the computation of the parameters used (modelST, modelET, modelSA, modSACT) for the polynomial fits.

Data that have been corrected for the very low frequency diurnal variations correlated with spacecraft phenomenon are archived in IFG and spacecraft coordinates in the "partially-processed" data collection (urn:nasa:pds:insight-ifg-mars:data-ifg-partially-processed). The data in this collection are provided for the purpose of decorrelating the high frequency signals observed by the IFG with those observed by the SEIS experiment. These data contain significant residual high frequency fluctuations that result from a combination of the natural environment and those attributable to variations in the spacecraft current systems (due to heater cycling, communication systems, etc.) which we collectively refer to as data artifacts.

3.2 Final Data Processing (v07)

While the previous versions of the data processing pipeline did a fairly good job of decorrelating the IFG magnetic field data with the various instrument temperatures and solar array current values, the coefficients did not seem physical. The coefficients from Equation 1 that defined the instrument temperature contributions ($C_{1,i}$ and $C_{2,i}$) showed large variations over short time intervals, and this is not the way that fluxgate magnetometers typically behave. Table 5 shows these variations for the B1_IFG axes over a few weeks time taken from the "PolynomialFits.txt file in the v06 document folder of the insight-ifg-mars (v06) bundle. The shaded the $C_{1,1}$ coefficient multiplies the sensor temperature and the $C_{2,1}$ coefficient multiplies the electronics temperature. Between April 24 and June 1, 2019 these coefficients differ by factors of roughly two and three in a little over five weeks (dark shaded cells). The reason for these large variations stems from deficiencies in our least squares method. The solar array current variations are highly correlated with the sensor temperature variations, at least during the daytime when the strongest magnetic signals are observed and we did not constrain the values of $C_{1,i}$ and $C_{2,i}$ in our fits.

Table 5: B1_IFG Polynomial Fit Coefficients for Equation 1 for calibrations up to v06.

Start Time	Stop Time	$C_{0,1}$	$C_{1,1}$	$C_{2,1}$	$C_{3,1}$	$C_{4,1}$
2019-04-24T20:30	2019-04-29T00:00	145.013	1.117	1.016	96.362	4.269
2019-04-29T00:00	2019-05-04T10:00	133.320	0.957	1.689	24.421	3.462
2019-05-04T10:00	2019-05-05T22:30	129.096	0.970	1.207	65.441	5.127
2019-05-05T22:30	2019-05-11T14:30	135.580	0.926	1.876	35.890	2.974
2019-05-11T14:30	2019-05-13T03:45	137.341	0.948	0.605	1.569	5.990
2019-05-13T03:45	2019-05-18T02:21	148.243	0.942	1.629	26.537	2.942
2019-05-18T02:21	2019-05-26T13:00	125.215	0.747	1.594	30.890	2.433
2019-05-26T13:00	2019-05-29T14:00	127.414	0.736	1.650	50.297	0.238
2019-05-29T14:00	2019-06-01T13:00	111.043	0.790	1.299	14.235	1.691
2019-06-01T13:00	2019-06-09T02:00	104.312	0.612	0.272	121.702	1.911
2019-06-09T02:00	2019-06-11T03:00	112.991	0.533	1.083	19.699	1.396

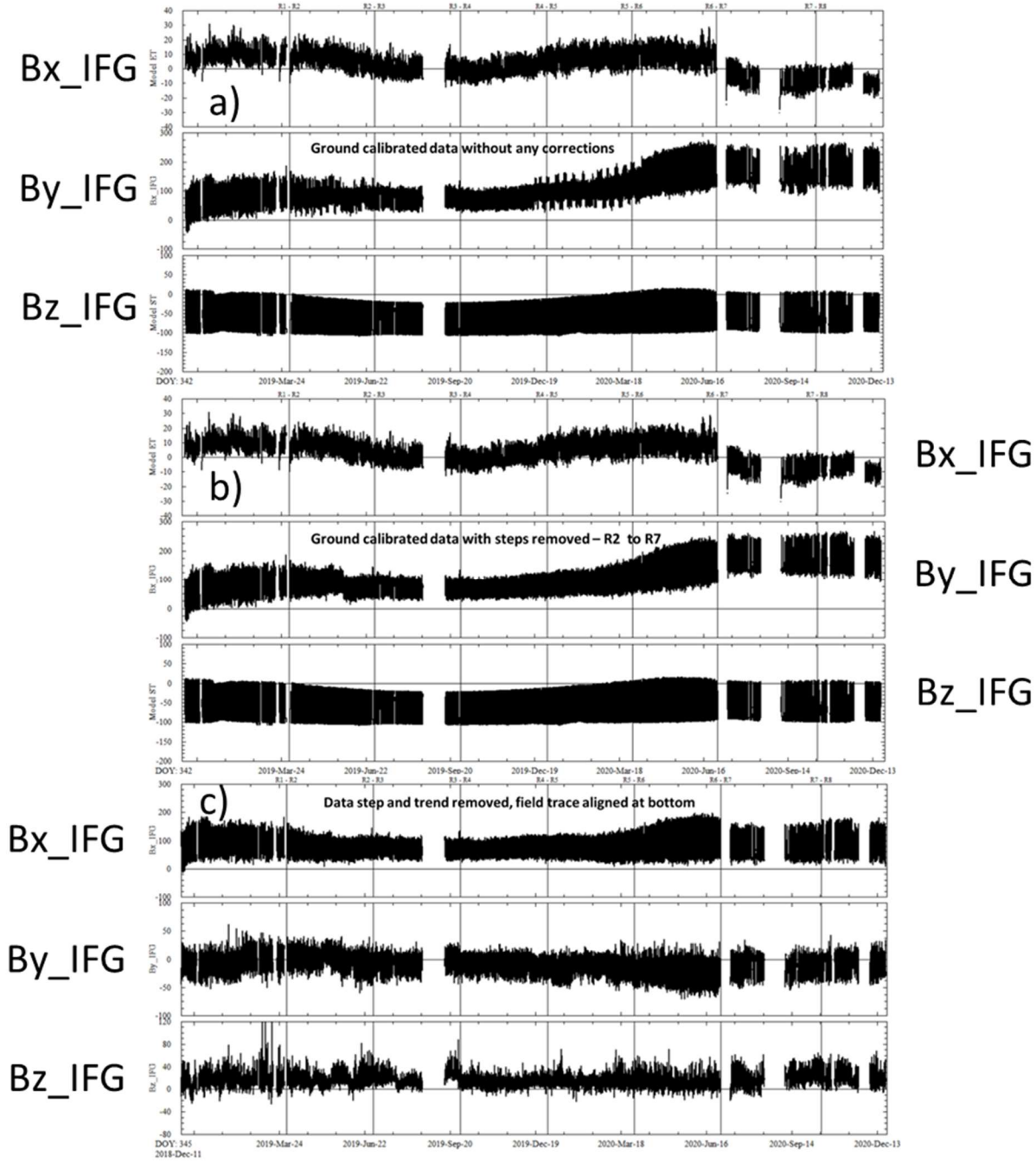

Figure 14: IFG dataset with ground calibration (a), after destepping (b), and after detrending (c).

The new approach was similar to the approach previously taken but designed to have the instrument temperature dependent terms remain constant over longer time intervals. We decided to separate the decorrelation process into a few steps, by first removing temperature effects and then removing the solar array current effects. Before we fit the field differences (dB_i) we needed to remove some spacecraft artifacts that are clearly not related to the instrument temperatures. These were typically large steps (5- 30 nT per component) in the data that persisted for days at a

time (documented in destep.txt) and long-term (seasonal) trends in the data. Figure 14 shows the complete dataset with just the ground calibration applied in the top panel (a), the data after step removal in the center panel (b), and after trend removal in the bottom panel (c). Release boundaries are shown on each panel. Each panel shows three traces which are Bx_IFG, By_IFG, and Bz_IFG from top to bottom respectively. dB's were computed from the destepped, detrended nighttime (henceforth called corrected GC) data and then fit with a linear function of sensor temperature.

To remove the temperature effects, we selected only "nighttime" data when there are no solar array currents in the corrected GC dataset. We defined night-time to be when the total solar array current was less than 1.5 Amp. The spacecraft reports a value of 0.075 Amps at midnight local time when there is clearly no sunlight on the arrays. We chose to allow a small amount of solar array current in our definition of nighttime in order to get a larger range of temperatures in the dataset to better constrain our fits. The temperature variation was computed by least squares fitting the sensor and electronics temperatures to the corrected GC data. The two instrument temperature variations are nearly ninety degrees out of phase so there is no need to fit them serially. We explored different duration datasets from 10 to 270 SOLs for our fits and found that a value of 90 SOLs or a normal InSight release worked well and was convenient for our existing data processing pipeline. In the documents folder of the newly processed archive bundle is a file called TemperatureFits.txt that gives the coefficients for the temperature corrections dB_temp_i (i=X, Y, Z) for each data release.

The temperature corrections were then applied to the full day corrected GC data to create the input dataset for determining the solar array current corrections. The amplitude and shape of the solar array current data changes frequently so these fits had to be computed piecewise as had been done in the earlier versions of the archive. These piecewise solar array current coefficients are included in the documents folder in the file called SA_Current_Fits.txt.

Since the data are processed one release at a time, special care had to be taken to make sure that there are no discontinuities in the data across these artificial boundaries. In general, this required some smoothing of the model temperature and solar array current values across the boundaries. In addition, the constants in the piecewise fits to the solar array currents had to be smoothed across the boundaries. Lastly, data from releases 10 to 14 were exceptionally sparse and it was difficult to determine temperature and solar array current corrections using only the data from that release. Coefficients from these releases may not be as well determined as those of earlier releases. Finally, much of the data during these later releases were acquired at night when data are typically quieter. This meant that there were few in any solar current values to use in the fits. While this may seem optimal, the solar array current fits are the ones that include the constants ($C_{0,i}$) that provides the baseline values. When this was the case, data segments were shifted up or down by adding or subtracting a constant to match the long-term trendline of the data.

Figure 15 shows the complete dataset plotted over two Mars years. The data in black are from year one (SOLs 1-668) and those in red are from year two [1]. Data are plotted versus MLST and 668 has been subtracted from the data in year 2 so that the data overlay. Later in the mission it appears that the variability of the data was less than in the first year. This is an artifact of the decision to preferentially acquire quiet nighttime data as can be seen in Figure 16. Figure 16 shows an expanded view of SOLs 530 – 580 with the true local solar time (TLST) plotted in the bottom panel. Horizontal lines have been drawn at 20:00 and 06:00 and it is clear that the red TLSTs traces fall between these bounds. The red field data traces from year two mostly overlay the black traces from year one. of SOLs 530 – 580 with the true local solar time (TLST) plotted in the bottom panel. Horizontal lines have been drawn at 20:00 and 06:00 and it is clear that the red TLSTs traces

fall between these bounds. The red field data traces from year two mostly overlay the black traces from year one.

Figure 15: Complete IFG dataset shown over two Mars years with the 2nd year in red. Year two data are shifted by 668 SOLs in order to overlay year one data.

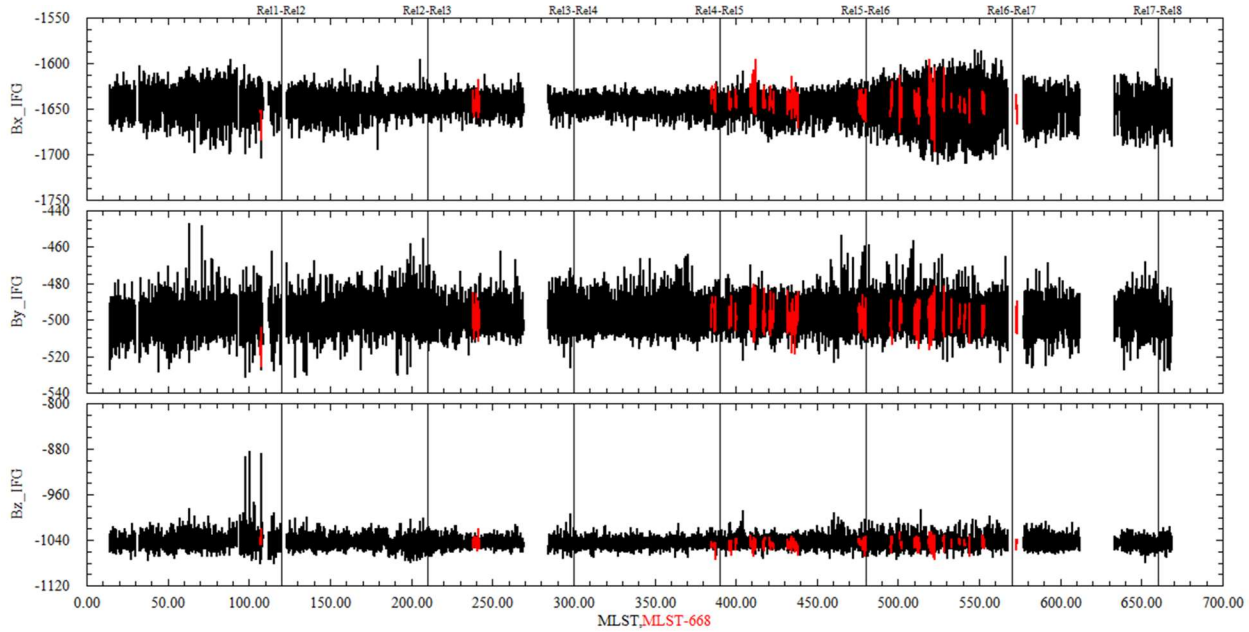

Figure 16: Expanded view of the Mars year overlay for SOLs 530 (1198) to 580 (1248). Year two data do not show the large daytime variations because they were mostly acquired during the Mars nighttime when the spacecraft was magnetically quiet and when short period waves had been observed [1, 2, 3].

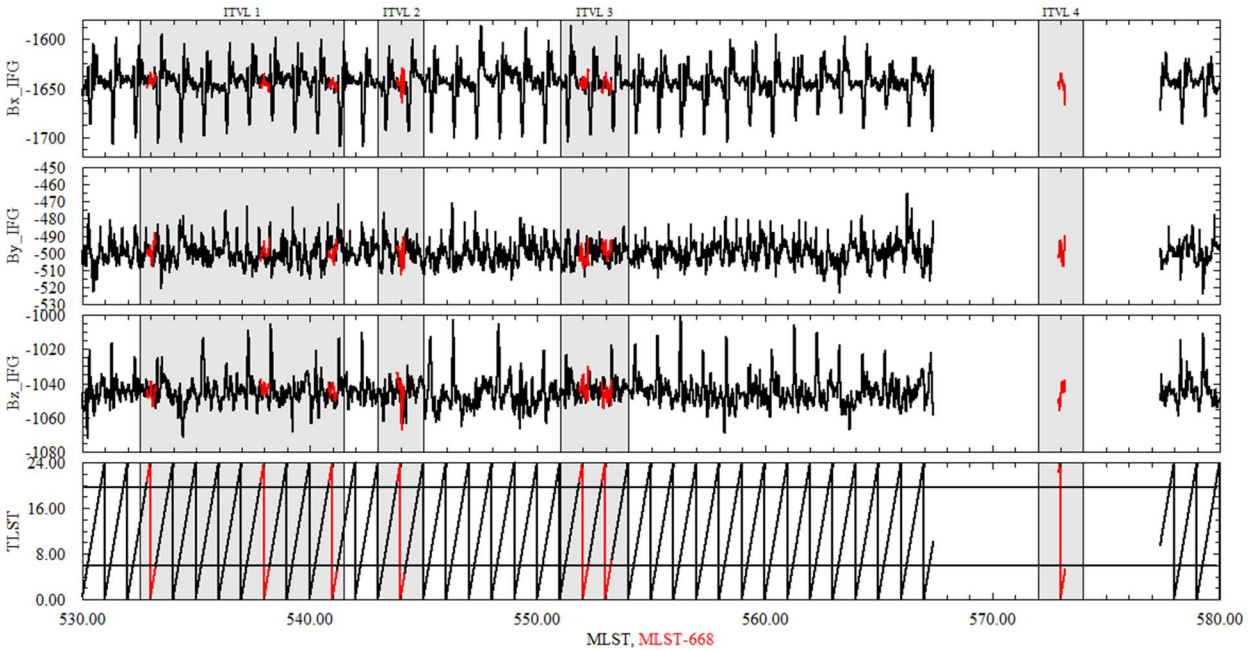

Lastly we show comparisons of the new v07 pipeline generated partially processed data to those previously delivered to the PDS. Figure 17 shows data from Release 4 with the baseline values (-1645, -500, -1045) subtracted so that the panels center on zero. In the top panel (a), the full release is shown with the PDS data in black, the new v07 processed data in green, and the difference between the two in magenta. Two time intervals are called out using yellow shading to identify a time period when the differences between the two datasets is particularly small, and in blue when they are large. In each of the expanded panels, the same color convention is used to identify data from the v06 and 07 data processing pipelines. The field values plotted in all three panels are Bx_IFG, By_IFG, and Bz_IFG from top to bottom respectively. In panel (b), the green v07 Bx and By traces nearly overlay the black v06 traces while the Bz traces show small differences in amplitude but show all of the same features. In panel (c), the Bz data mostly overlay and the Bx and By traces show differences. Again, the green traces show nearly all of the same perturbations as the black traces, with the same timing but with differences in the amplitude. Sometimes it appears as though the green trace could be shifted by a constant and match or nearly match the black trace, but any such shift would create shifts elsewhere in the dataset where none previously existed.

In summary, the IFG team believes that the new v07 data do not substantially change the overall characteristics of the data. This is the expected result. The main reason for the data reprocessing effort was not to make large changes in the dataset but to make the data processing algorithm more physically meaningful – to reduce the amplitude and frequency of the variation in the data attributed to instrument temperature effects.

Figure 17: Comparison of v06 (black) and v07 (green) partially processed data for Release 4 and their difference (magenta). The middle panel (b) shows an expansion of the time interval called out in yellow in panel (a) and the bottom panel (c) is an expansion of the blue time interval.

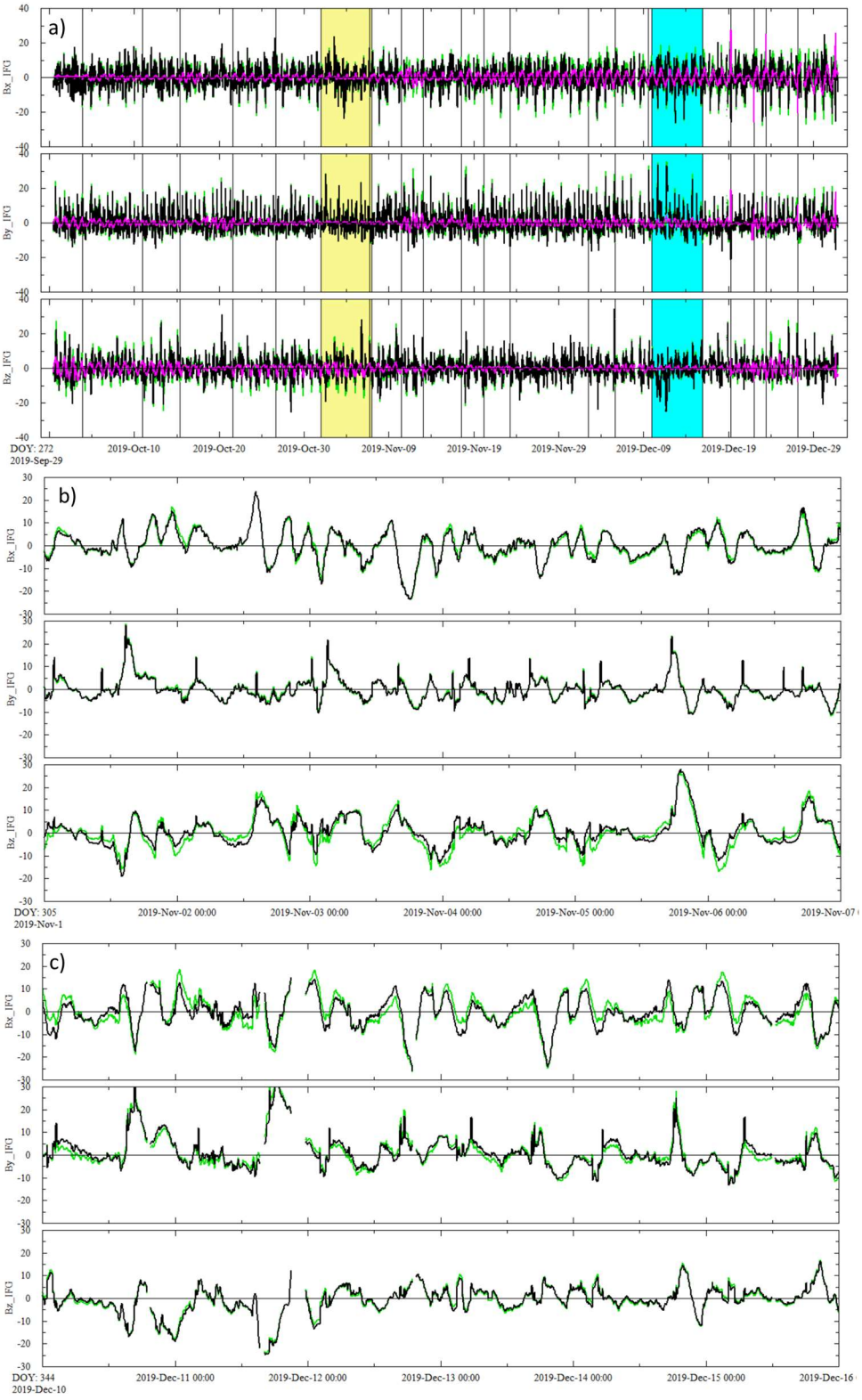

4 Data Artifacts

Prior to the first public data release, several types of artifacts were observed in the partially processed IFG data [4]. We have only been able to partially correcting many of these artifacts. The following sections describe the types of issues that are present in the data the uncorrected data.

4.1 Single Point Spikes

The first type of artifact found in the data that we will describe are single point data spikes. The source of these spikes is unknown although lander on/off changes is one source [4]. While spikes are observed in all components, typically only a single component is impacted at a time. Spike amplitudes are typically only a few nanoTesla.

Figure 18: Single point spike examples.

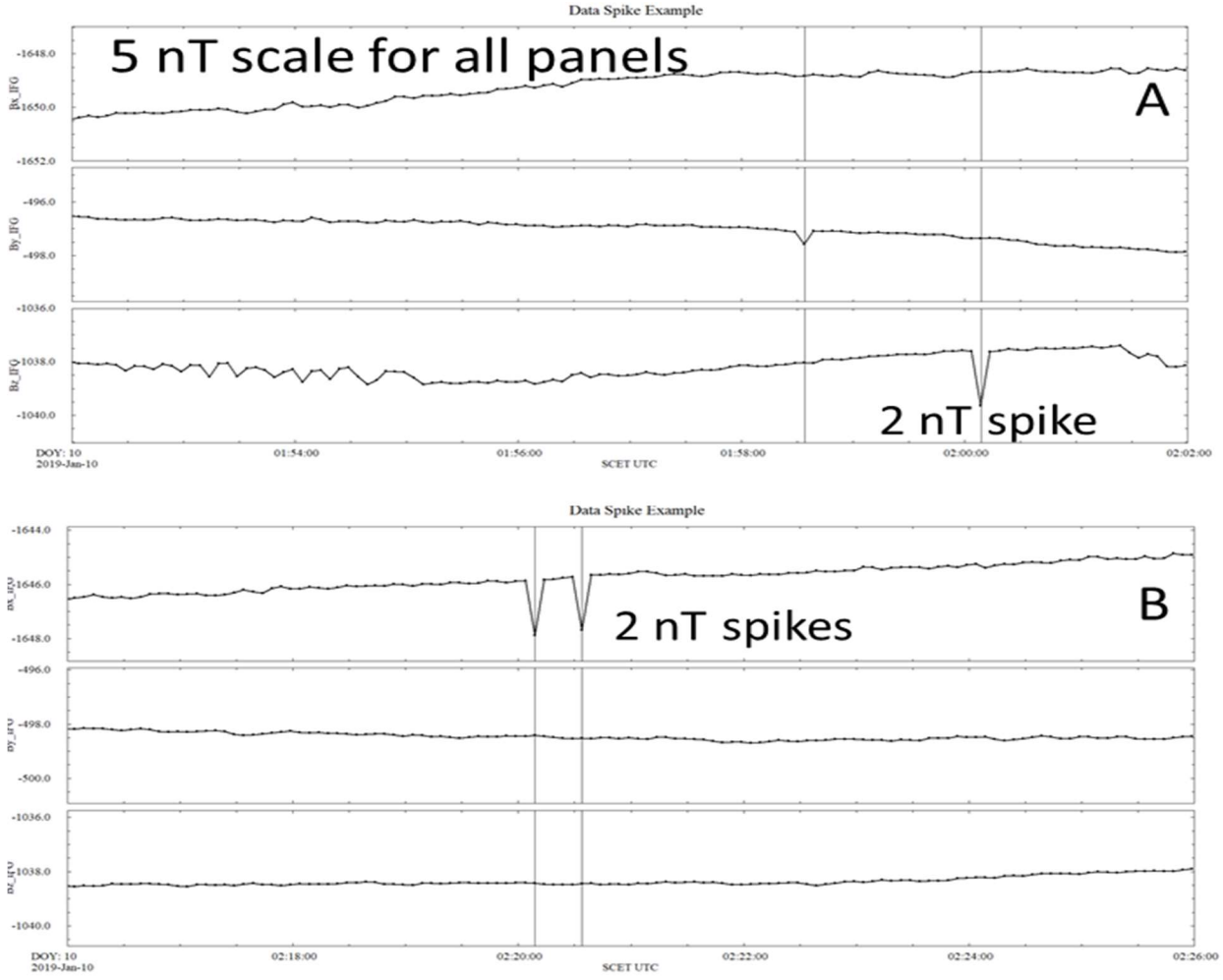

Figure 18 shows two examples of single point data spikes. Both panels show 10 minutes of data in IFG coordinates with a 5 nT scale and the actual data points shown as dots along the traces. In the top panel (A), there is an approximately 2 nT downward spike in the Bz component at 02:00:10 (vertical line) and another smaller fluctuation in the By component at 01:58:35 (vertical line). While the drop in the Bz component is large enough to be considered an artifact (spike), the

amplitude of the By component fluctuation is not. It is of the same magnitude as the Bz fluctuations that occur a few minutes earlier. The bottom panel (B) shows a pair of spikes of about 2 nT in the Bx component in close temporal proximity. Note that neither the spikes in the top or bottom panels occur in more than a single component.

Single point data spikes can be identified by comparing the value of a component sample to proceeding and following samples. If the sample differs more that some amount (1.5 nT TBC) from both preceding and following samples, and the preceding and following samples themselves do no vary by mode than some threshold (0.25 nT TBC), then the sample is identified as a spike and its value is replaced by the average of the preceding and following samples. Mathmatically, if

$(\text{abs}(B_{i,j} - B_{i,j-1}) > 1.5)$ and $(\text{abs}(B_{i,j} - B_{i,j+1}) > 1.5)$ and $(\text{abs}(B_{i,j-1} - B_{i,j+1}) < 0.25)$

then

$B_{i,j} = (B_{i,j-1} + B_{i,j+1})/2$

where the (i) subscript refers to the field component (1,2,3) and the (j) subscript refers to the sample number or time step.

Single point data spikes should be corrected/removed before attempting to identify or removed more complex interference structures. After identification and correction, the data quality flag (dqf) for the sample (8^{th} element from the right) should be set to 1 (Issue corrected in any/all components).

4.2 Square Wave Steps

Square wave steps are defined as intervals where two or more field components abruptly shift (increase or decrease) at the same time and then shift by approximately the same amount in the opposite sense sometime later. The sense of the shift (initial increase or decrease) is not same between components in general. Figure 19 shows two examples of square ware steps. In the top panel (A), the By and Bz components (IFG frame) shift in the opposite sense and then return to near their original levels after about 3 minutes. The shifts are small, roughly 0.8-1.5 nT in By and 0.5 nT in Bz. The negative enhancement of the By component at the onset is larger than the return at the termination. The same is true for the Bz component, although somewhat less apparent since the amplitude of the shift is smaller.

Panel B shows a much larger (7-10 nT in By and Bz, 1.6 nT in Bx) and longer (15:53 – 16:48) shift (shaded) that impacts all three components in the IFG frame that immediately following a shorter, smaller shift that is not shaded that primarily only impacts the By and Bz components

Figure 19: Examples of square wave steps.

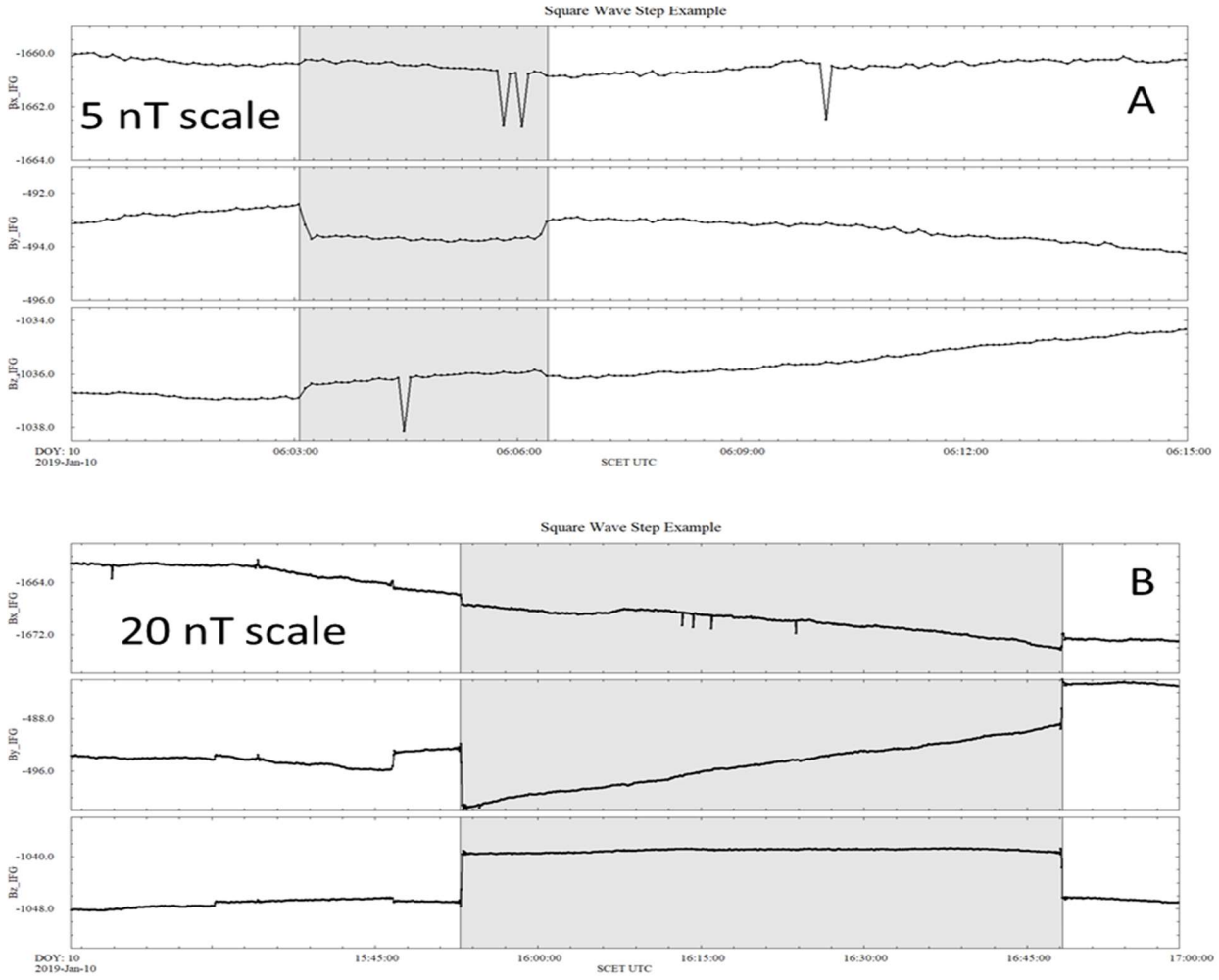

(~15:46). In both panels of Figure 19, the "step" duration is longer than the time between samples (5 sec) so that there is at least one sample part way between the top and bottom of the step. Square wave step identification and mitigation can be further complicated by short transient events near the onset or termination of the events. Figure 20 focuses in on the termination of the event show in panel B of Figure 19. In this figure you can see that there appears to be ringing of the FIR filter associated with the termination of this artifact. This ringing will complicate the determination of both the timing and amplitude of the artifact termination. Artifact removal may be incomplete or result in the introduction of additional artifacts. For the purpose of determining the amplitude of a potential step in a component, the differences between averages over five points, before ($B_{i,j-7}$ to $B_{i,j-2}$) and after ($B_{i,j+2}$ to $B_{i,j+7}$) the step is computed. This window needs to be small enough to not eliminate trends in the data and long enough to any filter ringing that might be associated with the step.

Figure 20: Blow up of the termination of a selected square wave step.

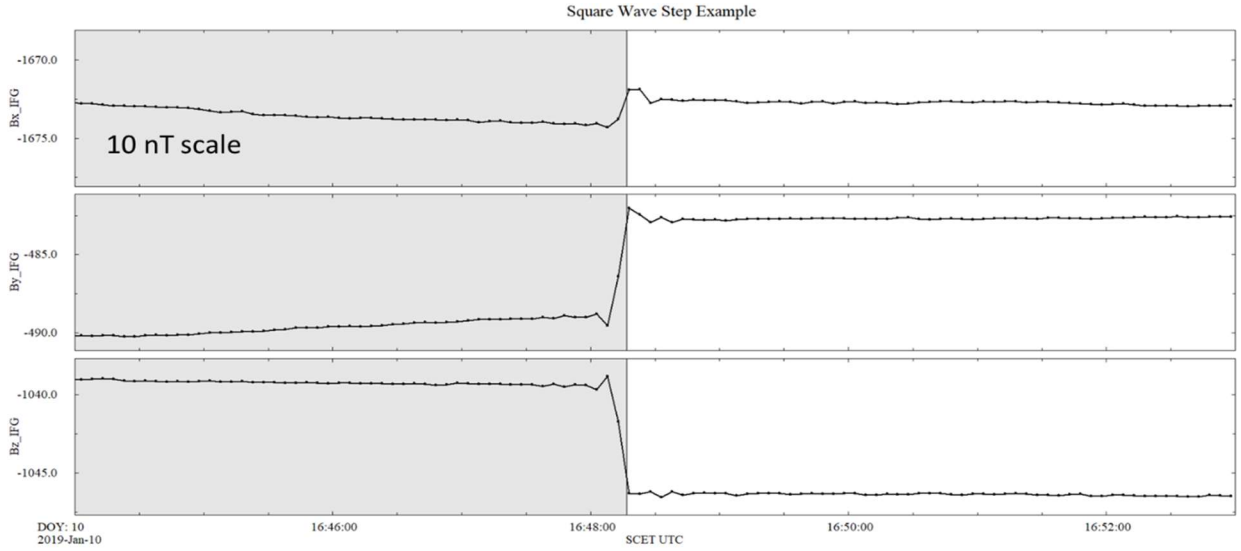

Square wave steps can sometimes be identified in an automated fashion by applying the following algorithm.

1) Onsets can be identified by comparing samples $B_{i,j-1}$ to $B_{i,j+1}$ where the subscript (i) indicates the component and (j) the sample time/number. The initial amplitude of the step at sample/time j ($A_{i,j}$) is $A_{i,j} = B_{i,j+1} - B_{i,j-1}$. If the absolute value of at least one initial $A_{i,j}$ is greater than 0.5nT – AND- the absolute value of the amplitude of another component ($A_{k\neq i,j}$) is at least 0.3 nT, then vector at time/sample j is a potential onset sample with step amplitudes of $A_{i,j}$. The onset sample (j) is recorded and the actual amplitudes are computed using the averaging method described above.

2) If a potential onset has been identified, then search for a termination sometime in the next 120 minutes by comparing samples $B_{i,j+n-1}$ to $B_{i,j+n+1}$ where (j+n) indicates a sample/time greater than (j) and the potential step amplitudes ($A_{i,\,j+n}$) are computed for samples (j+n). Potential termination steps and their amplitudes are determined as described for onsets. To be considered a step termination, the amplitude of the return steps must have the opposite sign as the onset amplitudes and be within 20% of the onset amplitude $-0.8 * A_{i,j} \leq A_{i,\,j+n} \leq -1.2 * A_{i,j}$ for all (i).

3) The identification and correction algorithms do their best to account for the "stacking" of events, as appears to be happening in the event identified in Figure 19, panel B where a second (or more) step(s) occur before the field returns to its unperturbed state. In this time interval, both the By (+2.9 nT) and Bz (-0.4 nT) components see a shift at 15:46 that would be identified as an onset event. It is unlikely that the slight shift in the Bx component (-0.2 nT) at this time would be considered since, given the downward trend in the data, the difference does not meet criteria (1) above. The potential termination event at 15:52 in components By (-9.5 nT) and Bz (+7.6 nT) amplitudes are too large to be identified as a termination, using the definition in (2) above. At this time, there is also a potential onset event in the Bx component (-1.6 nT). Since the events at 15:46 and 15:53 are not an onset/termination pair, they should be considered as separate onset events, and their amplitudes summed dBx = 0 - 1.6 = -1.6 nT, dBy = 2.9 – 9.5 = -6.6 nT, dBz = -0.4 + 7.6 = 7.2 nT. The next potential termination event occurs at 16:48 where there are shifts in all three components (1.8, 6.4, -6.9) nT. When the summed amplitudes of the onset events (-1.6, -6.6, 7.2) are compared

to amplitudes of the event at 16:48 (1.8, 6.4, -6.9), the termination criteria (2) are met. We refer to square wave steps that have multiple onsets as "compound square wave" events while those that have only a single onset and termination are called "simple square wave" events.

If a simple square wave event is identified, it can be at least partially removed by applying the following steps.

1) Begin by setting the values of the data immediately before and after the step to the average values used for the amplitude determination:
$B_{i,j-7}$ to $B_{i,j}$ are set to the average value of samples $B_{i,j-7}$ to $B_{i,j-2}$
$B_{i,j+1}$ to $B_{i,j+7}$ are set to the average value of samples $B_{i,j+3}$ to $B_{i,j+7}$
$B_{i,j+n-7}$ to $B_{i,j+n}$ are set to the average value of samples $B_{i,j+n-7}$ to $B_{i,j+n-2}$
$B_{i,j+n+1}$ to $B_{i,j+n+7}$ are set to the average value of samples $B_{i,j+n+3}$ to $B_{i,j+n+7}$

2) For samples (j+1) to (j+n), the linearly varying amplitude between the onset and termination is subtracted from the field components. The linearly varying amplitude can be represented as
$linAi,k = Ai,j + dAi,k$
where k=j, j+n and $dAi,k = (k-j)*(Ai,j+n – Ai,j)/n$ and the correction to field components is:
$Bi,k = Bi,k – linAi,k$ and the data quality flag for the square wave step element (9^{th} from right) should be set to reflect partial correction of more than one component for samples between (j-7) and (j+n+7). The dqf value for this offset should be set to 2 (all components partially corrected) if the step was identified in all 3 components. The dqf value should be set to 3 (partially corrected in more than one component) if the step was only identified in two components.

If a compound square wave step is detected, the mitigation follows the same steps as for a single step except that the linear variation in the step amplitude from initial onset to termination needs to be distributed across the total event duration. For simplicity, we will only describe the mitigation of the event shown in Figure 19, panel B. We use the sample subscripts (j, j+n, j+m) to describe the steps at 15:46, 15:53, and 16:48 respectively and call the amplitudes at the step A1, A2, and A3. Amplitudes A1 and A3 are computed as described above for a single step. Amplitude A2 is the difference between A3 and A1 ($A2_i = A3_i – A1_i$). In this example, the step in Bx at 15:46 is zero ($A1_1 = 0$). The linear drift rate ($dA_{i,k}$) for components By and Bz is computed from the time of the initial onset to the termination (j, j+m) while for Bx, it's computed between (j+n,j+m). By and Bz samples between the first and second onsets (j+1 to j+n) are corrected using $A1_i$ and $dA_{i,k}$ (k=j+1, j+n) and those between the second onset and the termination are corrected by using $A2_i$ and $dA_{i,k}$ (k=j+n+1, j+m). In this case, the dqf value is set to 3 for sampled (j-7, j+n-7) and to 2 for samples (j+n-6, j+m+7). The values of Bx are unchanged until sample (j+n-7) so only two components have been corrected prior to this time. Bx values between (j+n-7, j+n) are corrected during the computation of $A2_1$ so the dqf for these samples should reflect partial corrections to all 3 samples.

Automated identification and removal of square-wave and compound square wave artifacts has had limited success. Steps that are abrupt and whose onset and termination amplitudes are very similar are removed by our processing. However, a large number of artifacts remain because one or more of these conditions is not met.

4.3 Square Wave Steps with Bounding Fluctuations

One of the more complicated forms of data artifact is referred to as a square wave step with bounding fluctuations. As its name implies, these artifacts appear similar to the simple or compound square wave but the determination of the step size at any or all steps is complicated by fluctuations near the steps. Figure 21 shows examples of some events. In panel A, sharp steps occur in the By and Bz components that are either followed by or preceded by field fluctuations that are not sinusoidal (shaded region). At the same time, there are drops and fluctuations in the Bx component that are not abrupt at onset or termination. In this example, the fluctuations are positive and negative excursions from the shifted trend lines. In panel B, there is a small, simple square wave onset in By and Bz, followed by a second step that begins with fluctuations. In this example, the fluctuations appear to be variations between the initial and shifted trend lines. In both panels, the data plots have been annotated with a blue line that shows the likely field trend in the absence of these artifacts. However, the IFG team was unable find an algorithm for the detection or correction of these events even though they are easy enough to detect by visual inspection. Any correction algorithm will likely involve removing of the steps and fluctuations as separate actions. If the fluctuations are removed from the data, extreme caution will need to be exercised to prevent the unintentional removal of fluctuations of geophysical interest.

Figure 21: Square wave steps with bounding fluctuations.

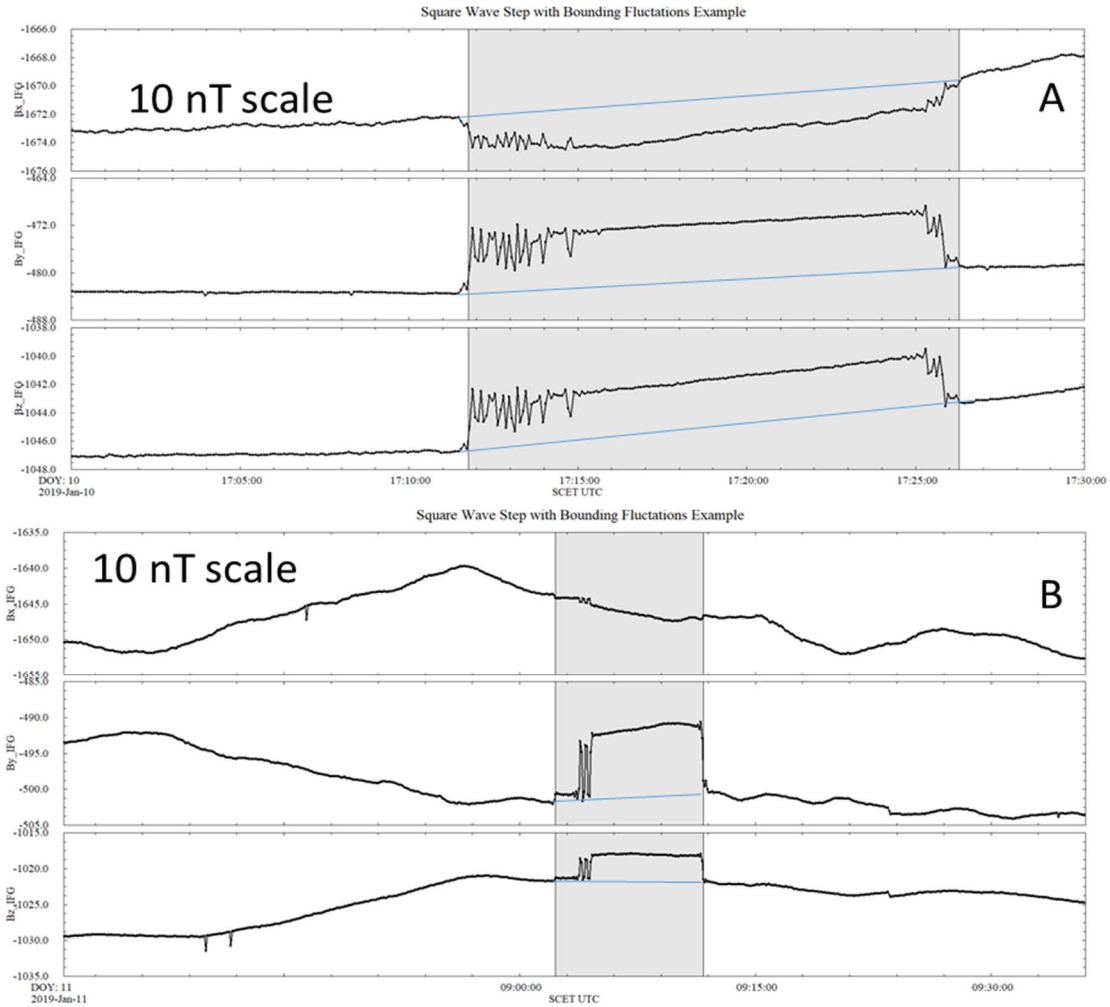

4.4 Irregular steps, ramps, etc. between 11 and 12.5 hours TLST

The artifacts discussed thus far can occur nearly any time of day on Mars, although nighttime is generally much less impacted than the daytime when the other payload systems are active. This next type of perturbation occurs regularly near mid-day TLST. Figure 22, panel A shows four Mars days of data with the TLST time period between 11 and 12.5 hours shaded in each day. In each of these shaded intervals, you can see a disturbance that is strongest in the Bz component. Panel B expands the time interval on February 5, 2019 so that the types of variations can be shown in more detail. The TLST interval from 11-12.5 hours is shaded and there are some vertical lines are drawn to guide the reader's eyes between panels. On this day, the interference begins at 11.2 hours and ends at 12.1 hours (first/last vertical lines). Over the entire interval,

Figure 22: Irregular steps, ramps, and other fluctuations between 11 and 12.5 hours TLST.

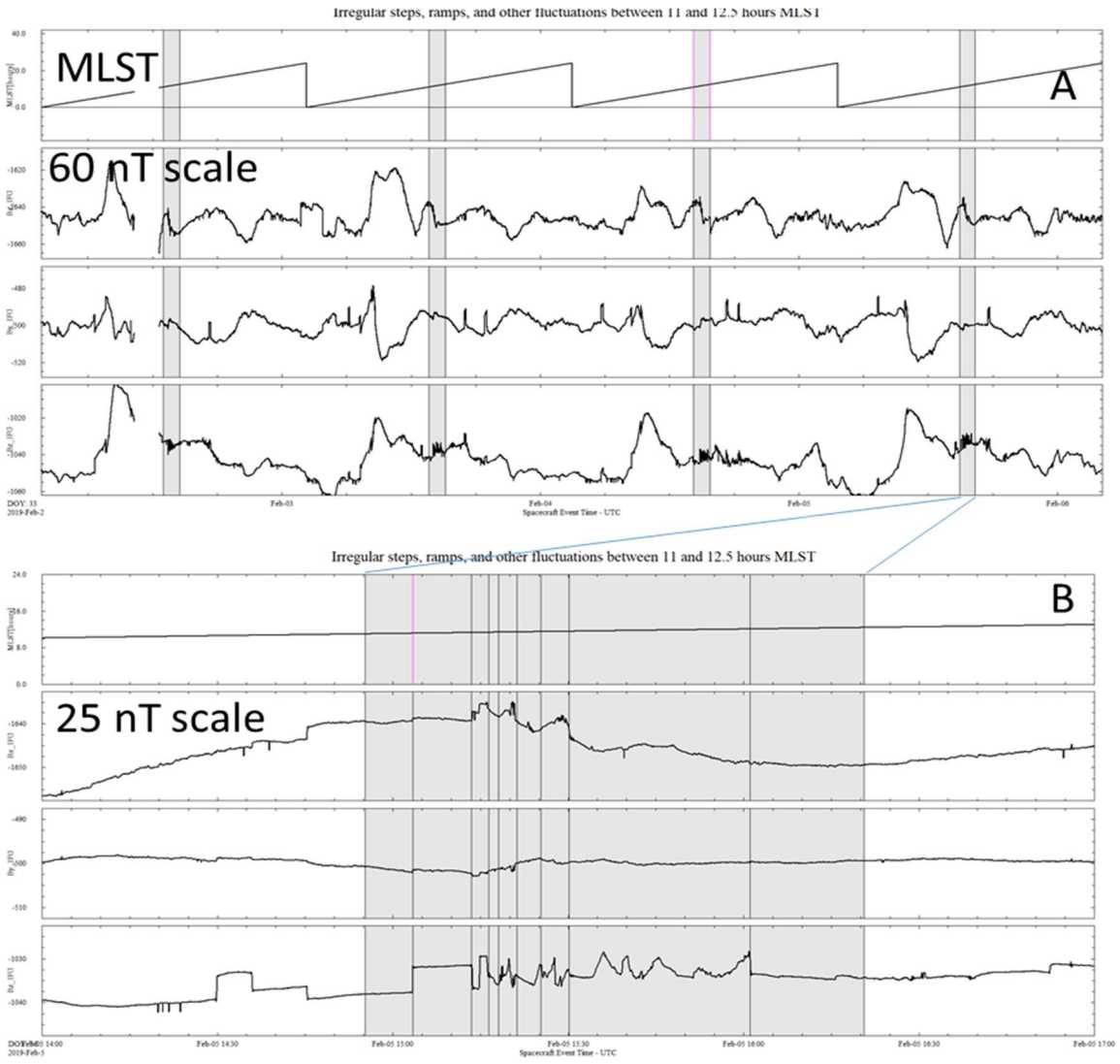

there is very little disturbance in the By (IFG) component, and a lack of participation in these events is characteristic of this type of disturbance. There are fluctuations in the Bx component at the times of some of the changes in the Bz component, but not for all of them and the shapes of the fluctuations are not necessarily the same. This is also common for disturbances in this TLST time interval. Many of the Bz fluctuations look more like ramps or humps than steps or spikes. It is unlikely that these types of fluctuation will ever be removed from the data unless a current system on the spacecraft can be found to have shapes to these similar to these signals and the parameter is available in the spacecraft engineering and ancillary data (SCEA) at a cadence that is sufficient to resolve and remove the magnetic signatures. Typically the SCEA data have both low cadence and low continuity on this spacecraft making them very difficult to use directly for the removal of spacecraft artifacts from the magnetic field data.

4.5 Large, long duration compound steps

Figure 14 shows examples of the long duration steps that needed to be removed from the data before they could be fit to new functions of temperature and solar array currents over the entire mission. Here we look one such event in more detail. These events and their corrections have been touched upon briefly in the SIS in section 3.2.3.4 (Raw to Partially Calibrated Data Procedure) and are described in detail in the *destep.txt* file. As discussed in Thorne et al. [4], these artifacts are associated with various lander activities, and communication activities in

Figure 23: Large long duration step in January 2020

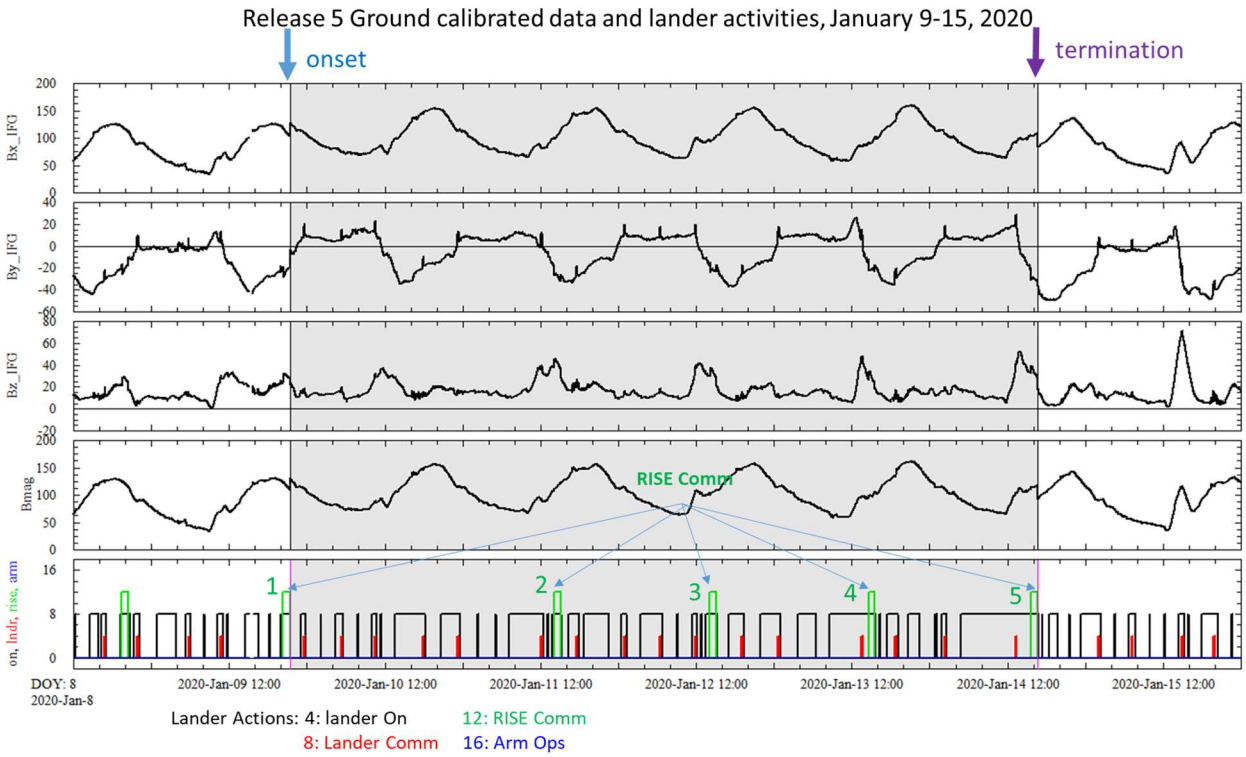

particular. Figure 23 shows an example of one such event in January 2020 along with various lander activities that were occurring at the same time. The main step (shaded interval, dBx = -21.66 nT, dBy = -12.65 nT, dBz= -3.22 nT in the IFG frame) with it's onset and termination are identified and both appear to be correlated with the completion of a RISE-COMM communication (green trace, bottom panel). Figure 24 shows several components of the event in

greater detail. Each panel contains traces for Bx, By, Bz, and |B| in the IFG frame with the bottom trace being the lander activity (LA). Vertical fiducial lines have been drawn at some of

Figure 24 Long duration compression and association with lander activities.

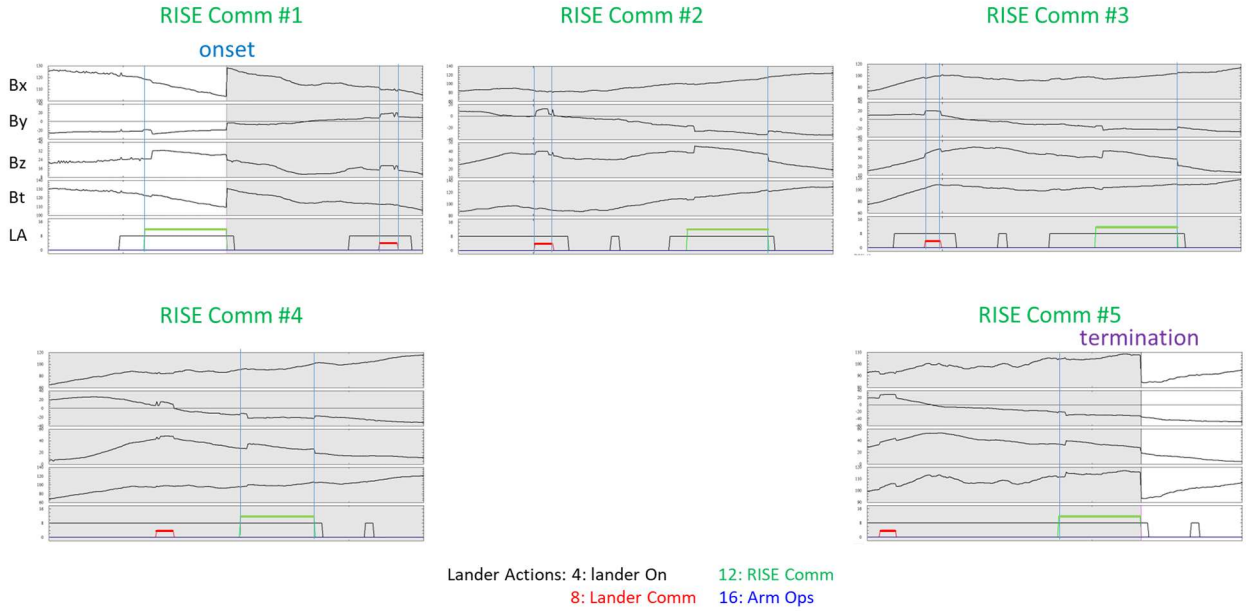

the start/stop of various lander activities to show their correlation with field disturbances. In general, there are small rotations approximately about the IFG X-direction loosely associated with the RISE -COMM and Lander-COMM communication modes (dBx too small to see at this scale). The rotations associated with the RISE-COMM mode begin after the mode change but end at the same time. Those associated with the Lander-COMM mode are more or less coincident with the field rotations. The large compression in the field appears to be coincident with the ends of the rotations associated with the RISE-COMM modes labeled RISE COMM #1 and RISE COMM #5. The IFG team is not aware of anything that might be special about these two RISE-COMM events.

4.6 Other artifacts

Many if not most of the artifacts that remain in the 0.2 Hz and 2 Hz data have been described above. However, there are other types of artifacts that are found occasionally throughout the data set.

Several different artifacts are identified by shading and probably trend lines are shown with blue lines, although other markings are also present. Starting from the left side of Figure 25, the first shaded region shows a set of downward ramps in the Bz component with no corresponding variations in the Bx or By components. The vertical line in this shaded region shows a return to trend followed by another ramp down the sharply returns to the trend after a minute or two. Moving to the right, the next shaded region shows a sharp step in the Bz component that returns to the trend after a few minute. However, during the disturbed interval, Bz does not follow the trend so this can't be described as a square wave step. There are no deviations from the trends in

the Bx or By components at the onset of the artifact but both components show variations at its termination. The Bx component has a step (circled) at this time with no clear step back to the previous level at a later time. It may be that the red line shown represents the trend in Bx and

Figure 25: Various other types of artifacts.

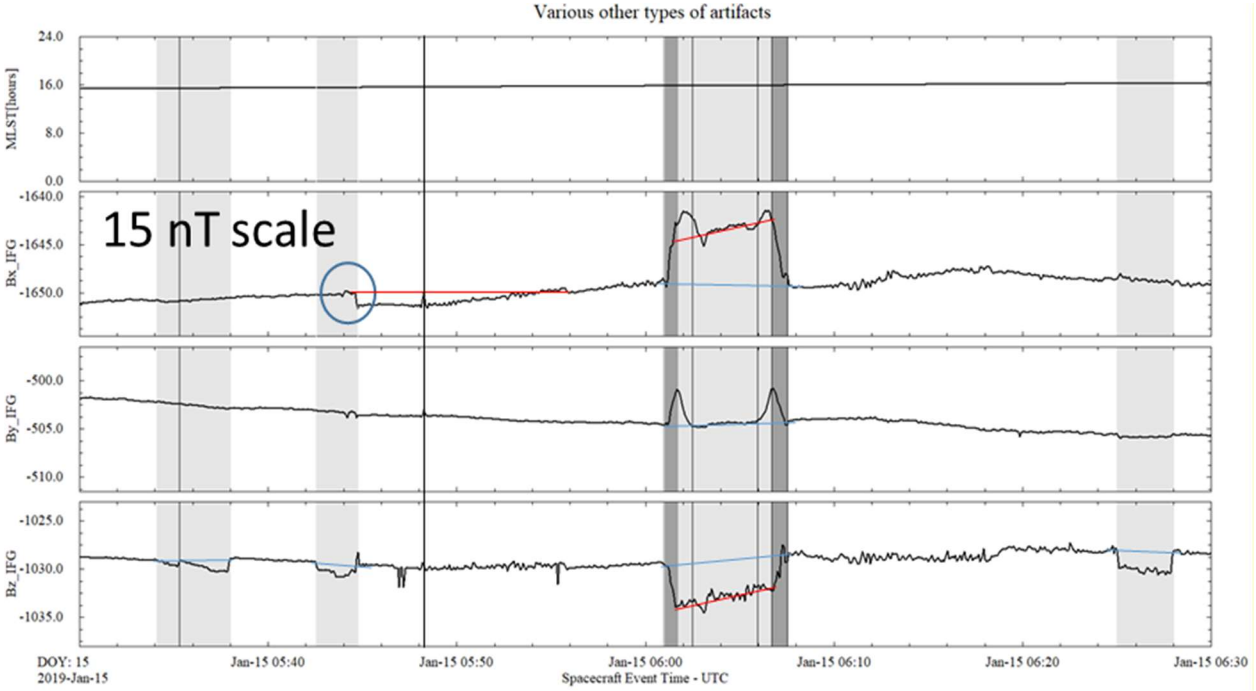

that there is a slow, ramping back to the trend over the next 8-10 minutes, however this is purely speculative. During the middle of this event, there is a brief excursion of the Bx component back to the putative trend line marked with a vertical line. This excursion involves 5 or six data samples, unlike the single point spikes that occur between 05:45 and 05:55 in the Bz component. In addition, there are small fluctuations in the Bz and By components at the time marked by this vertical line. Moving to the next shaded region, there is a fairly sharp drop in the Bz component over several data points, followed by a return to the trend 5 or 6 minutes later. However, the onset and termination steps are different sizes and the slope of data within the disturbed region (red line) is greater than that of the trend line. The By component shows a field increase and decrease of about the same duration as the drops/rises in the Bz component (dark shaded regions) but the field returns to trend in the middle of the Bz disturbance. The disturbance in the Bx component has features that are correlated in time with those in the Bz and By components, including the slope of central trend line (red – parallel to red line in Bz), but are otherwise different from the signatures in the other two components. Moving on to the last shaded region, the appears to a square wave step that only affects the Bz component. While there might be very slight variations in the other two components at the onset and termination events, these would not be identified by the previously stated identification criteria. Clearly there are many different current systems active on the spacecraft during this time period, each of which has its own magnetic signature and the observed field variations are the sum of the contributions of the individual currents. It is unlikely that any automated identification criteria or mitigation algorithm can be developed to flag and/fix any of

these types of events in the data. We can only hope that once the spacecraft is fully commissioned, disturbances such as these will no longer be observed in the IFG data.

DQF value for the 2^{12} place was initially designed to identify the types of long duration steps that had been observed in Release 1 data. However, when additional data were acquired and the nature of the artifacts demonstrated significant variability, the decision was made to not use this flag. Its value is always set to 0 in the data files. Users are referred to the "destep.txt" file in the document collection to see what if any corrective actions have been taken.

4.7 Artifacts in the high time resolution data

Thus far, the artifacts that have been described have been restricted to those that are identified in the low time resolution (0.2 Hz and 2Hz) continuous data. Data are available at higher data rates for selected time intervals when the downlink bandwidth allowed. All of the artifacts described previously are present in the high time resolution data, although the signatures may be slightly different in terms of onset or termination durations. One phenomenon that is present in nearly all of the high time resolution data is the toggling of the samples between multiple, parallel, baseline values, as shown in Figure 26. The top panel (A) shows five hours of 20 Hz resolution data at a fixed 60 nT scale while the bottom panel (B) zooms in on two minutes of data near the onset of persistent toggling. Panel (A) shows that the onset of the toggling is very rapid, and that Bz is the component that is most severely impacted. The data in panel (B) are displayed at different vertical scales in order to show that similar phenomenology is occurring in all of sensors at different amplitudes. Blue trend lines have been overlaid on the data in panel B to guide the reader's eyes. Focusing on panel (B), and starting on the left side of the figure (07:42:00), the magnetic field appears to have a baseline of about (-1670, -507.5, -1050) nT with spikes of different amplitudes on the order of a few nT around this value. At approximately 07:42:35, the field begins to toggle between values at the existing baseline and a new baseline of (-1668, -507.0, -1043) nT. A few seconds later, a 3rd baseline value (-1047) appears in the Bz component. A third baseline appears briefly in the Bx component (-1666 nT) at around 07:42:50. Eventually the field gradually begins to stabilize around a new baseline value of (-1668, -507.5, -1047) at around 07:43:50 leaving By unchanged. As panel (A) clearly indicates, this is only a brief hiatus in the toggling, while panel (B) demonstrates that beneath the hash, baseline changes are occurring.

If these fluctuations occurred with step sizes that were integer powers of two in the raw data, they would look like bit flips between two states in one of the middle bits (2^7 - 2^{11}) in the 24 bit analog to digital conversion, of the type that are always present in the lowest order bits in digital data. However, this is not what is happening. The sensor scale factors are all near 140 so that 140 DN (data numbers) approximately equals 1 nT, The observed step sizes require several bits to toggle in the middle registers simultaneously. While suspicious in appearance, this is not an instrumental artifact.

IFG team tried several algorithms but was unable to remove the toggling fluctuations from the high rate data in the normal data processing pipeline.

Figure 26: High time resolution toggling near a baseline step.

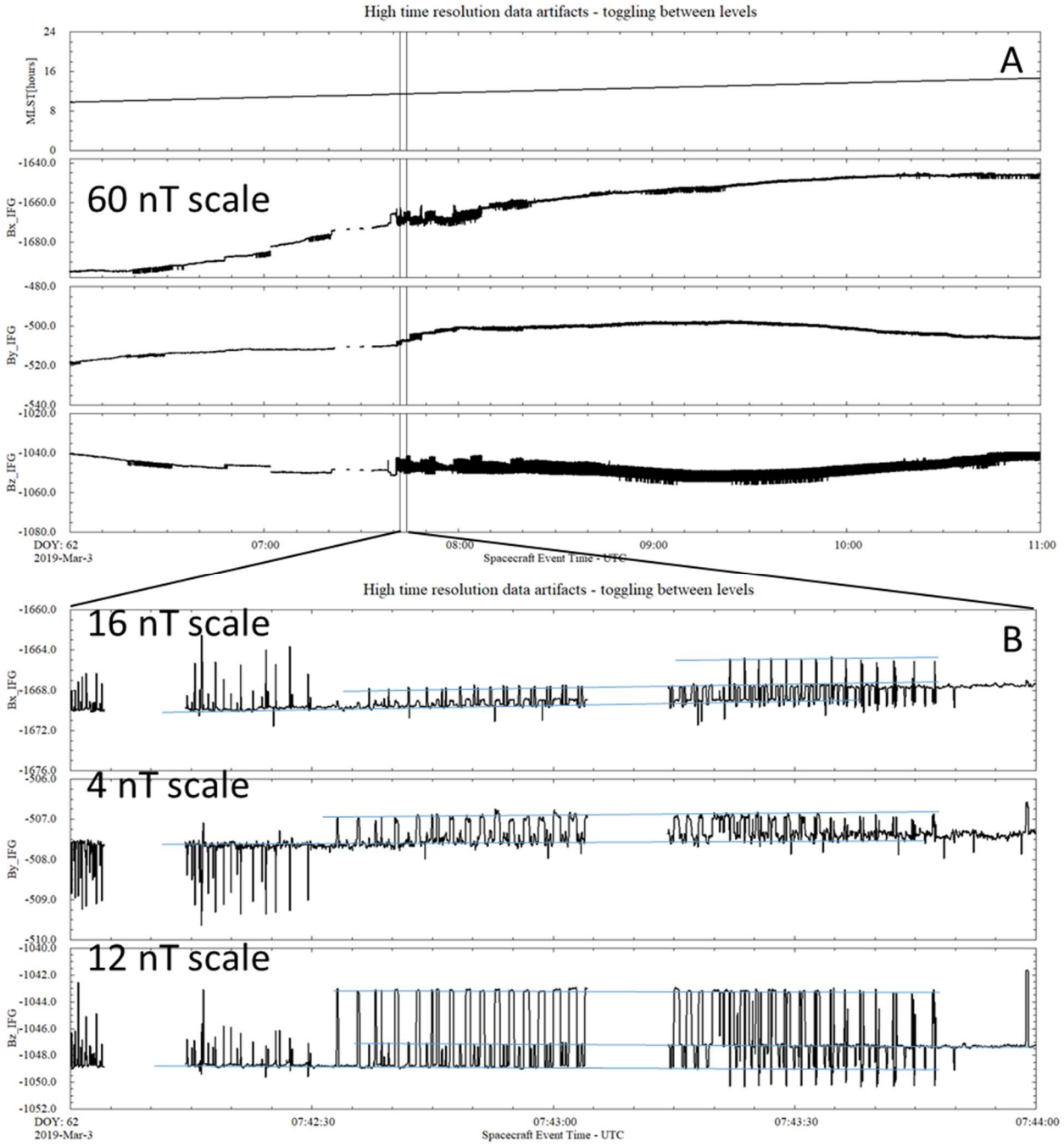

5 20Hz MAVEN Fly-over Data Collection

The v07 bundle contains a collection of 20 Hz data files that are subsets of some of the files that are provided in the "calibrated" data collection. Since the number of files is fairly small, the IFG team did its best to clean the data by hand to remove artifacts such as steps and minor toggling. Some of the files (24 of 98) were so badly corrupted that hand processing was only used to correct steps in the data and not the toggling. As discussed in the SIS, the most badly corrupted data were additionally cleaned by first subtracting 5 point running medians from the hand-cleaned data files. This process removes most of the toggling but also reduces the frequency content of the data files. Adding 1000 point running medians of the hand-cleaned data to the data files restores the field magnitude and low-frequency content of the data files.

Figure 27 shows an example of some hand-cleaned data from SOL 254. The red trace shows the data as it is in the calibrated data collection. The black traces shows the results of the hand cleaning. Most of the steps in the data have been removed, as well as the limited amount of toggling that was present in the data. The hand-cleaning process consists of identifying the start and end of impacted regions and then adding or subtracting a constant from the data in spacecraft coordinates. Many of the steps occur over several data points in the 20Hz data. When this occurs, the cleaning process creates small spikes in the dataset. The spikes are removed by comparing the data to 20 point running medians and samples that deviate by more than 0.2 nT are replaced by the median values at that time. The despiking process creates bad values at the beginning and end of the time intervals as well as at the edges of data gaps (incomplete buffers). To correct these bits of data, the edges of the data are additionally cleaned by repeating the values of the first uncorrupted data values and adding 0.1 nT of random noise.

Figure 27: MAVEN flyover, SOL 254 before (red) and after (black) hand cleaning.

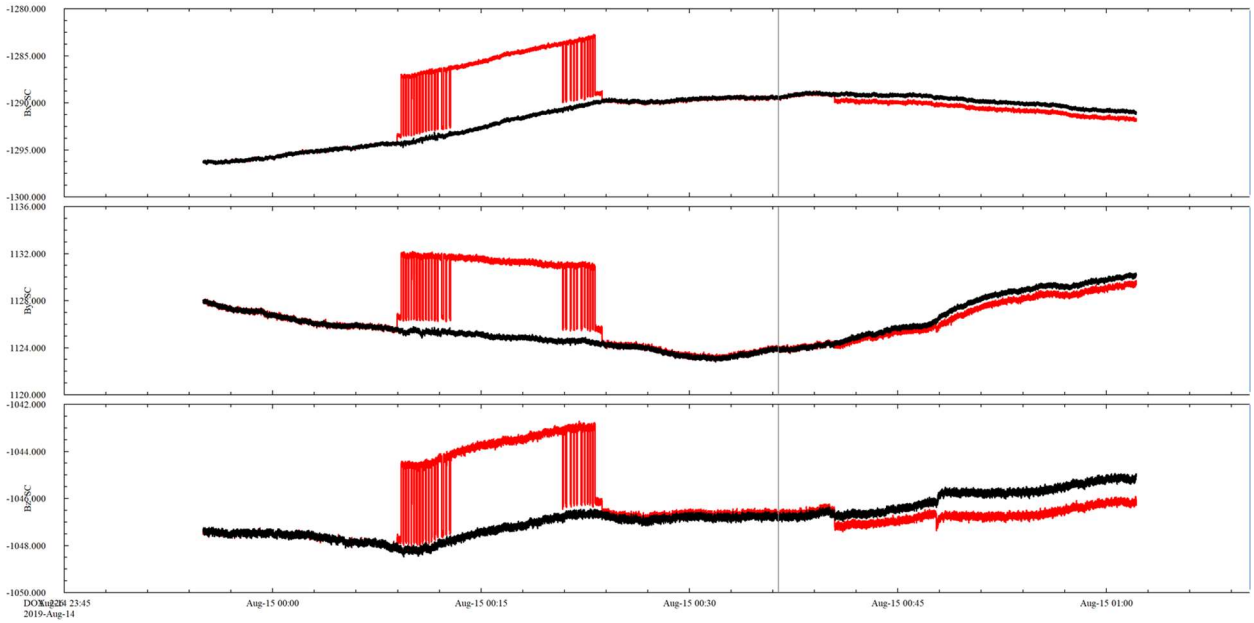

Figure 28: Close-ups of residual artifacts of hand cleaning.

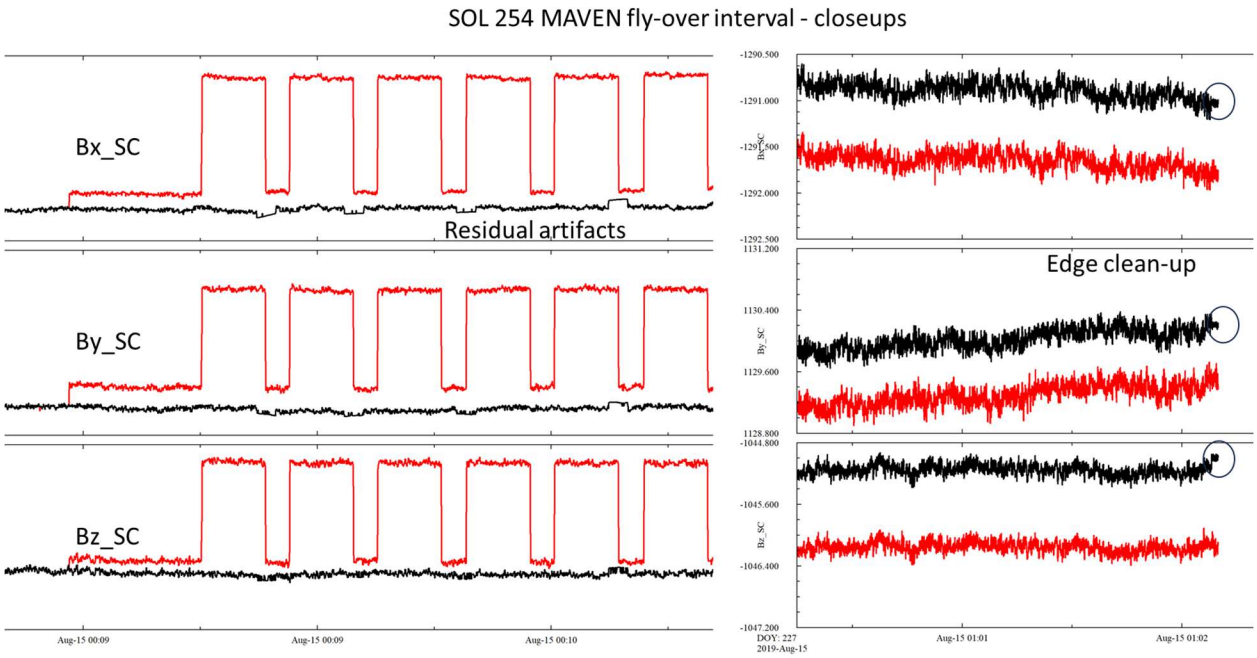

Figure 28 shows that even after cleaning, artifacts remain in the data so users should use caution when analyzing these data. Additional cleaning may be appropriate for some applications to remove artifacts around toggle corrections. For this SOL, it appears as though a larger amount of random noise may have been appropriate in the edge corrections interval. Not all MAVEN flyover intervals have as much noise as SOL 254. The 0.1 nT value was selected to match the quietest observed interval. Edges can be trimmed if the data are not needed.

Figure 29 shows an example of data where thorough hand cleaning was not feasible so the median cleaning approach was applied. The black traces shows the original data and the red traces show the median cleaned data. Long duration steps are still removed from the data by hand before median cleaning is applied.

Figure 29: MAVEN flyover data before (black) and after (red) median cleaning.

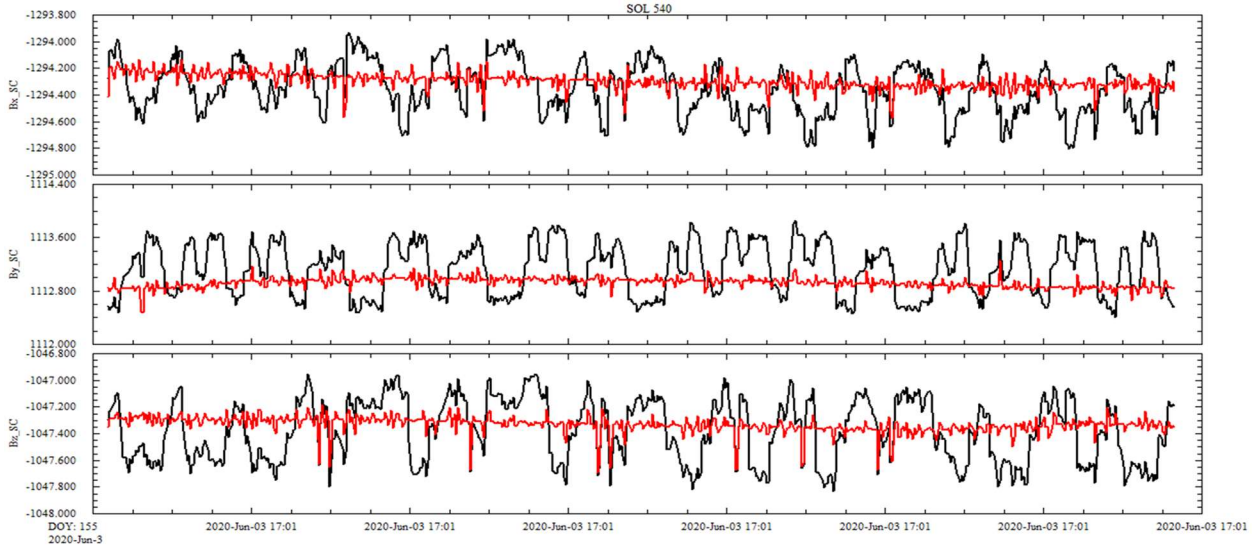

6 Data Pipeline Versions and Documentation updates

6.1.1 Versions in File Names

PDS assigns a version to each product in the archive as discussed in InSight IFG SIS Section 4.5.3 VID Formation. However, the version number that the IFG team assigns to the files that are provided internally and then archived reflects the version of the data processing pipeline used to create the data. IFG and spacecraft engineering data have separated data processing pipelines. The latter hasn't changed and is, and likely always be, version v01. The IFG data processing pipeline has gone through several versions which are described below.

6.1.1.1 IFG pipeline version v01

Initial version, mostly used to process cruise data and data shortly after landing. This version assumed that AOBT=SCLK for UTC time conversion. In addition, since sensor and electronics temperature values were sparse or unavailable, models of these temperature variations were developed and used for calibration.

6.1.1.2 IFG pipeline version v02

UTC time tags correctly computed by properly accounting for the AOBT drift relative to SCLK. Removal of the diurnal variations in the data correlated with solar array fixed and total currents was added. Models of temperature and current variations were replaced by polynomial fits to these values in order to track temporal variations in the MLST signatures.

6.1.1.3 IFG pipeline version v03

An error in the time tag associated with the IFG sensor temperature values was discovered and corrected. This error most strongly affected data acquired between about 06:30 and 09:30 MLST when the temperature was rising quickly.

6.1.1.4 IFG pipeline version v04

An initial version of a data spike and square-wave step removal process was added to the calibration procedure of the 0.2 Hz data in spacecraft coordinates. These features remain in the partially processed data. The difference between the values of (Bx_SC, By_SC, and Bz_SC) in the calibrated versus partially processed data is the correction that has been applied.

6.1.1.5 IFG pipeline version v05

An error in the temperature and solar array current column orders occurred in the v04 during release 2. This error was corrected in release 3, v05. Since the impacted columns do not exist in the calibrated data the version number of this pipeline was not incremented.

6.1.1.6 IFG pipeline version v06

Prior to pipeline version v06, the column in the data files labeled MLST actually contain TLST values. This error was discovered in late April, 2020. After some internal discussion, the IFG team decided that the best path forward was to include both local times, mean and true, in the data files and to redeliver to the PDS all data to date with the value in the MLST column correctly computed. This error did not impact the ancillary data files.

6.1.1.7 IFG pipeline version v07

The v07 pipeline changed the way that instrument temperature and solar array current corrections were applied to the data. In addition, there was a lot of work put into cleaning up the model temperature and SA current values used for these corrections. Since the raw data products include

these model values, new raw data products are provided in the v07 delivery. A new bundle was created (insight-ifg-mars-newcal) and data from the entire mission were reprocessed using the v07 data pipeline. There are no changes to the spacecraft engineering data so these products are only included in the new bundle as a secondary data collection.

Appendix 1: IFG Sensor Temperature

In general, when the IFG is on and acquiring data, the sensor temperature data are available. The exception occurs immediately after a power on or PAE reset. The FIR filter applied to the temperature data is much longer and it takes more than two hours for the first sensor temperature sample to be output. In order to be able to process the IFG data in the absence of temperature data, a model of the temperature versus MLST has been developed. To develop the model, sensor temperature data from December 16-31, 2018 were binned into 0.1 hour MLST bins. The binned data were then fit using a polynomial function of MLST. In order to make sure that the model was continuous across the 24 to 0 hours MLST boundaries, data from the 22-24 hour bins were duplicated as hours -2 to 0, and similarly, the data from hours 0-2 were replicated as hours 24-26. Binned data from the MLST range -2 to 26 were then fit. The shape of the temperature variation over the Mars day could not be fit with an acceptable error by using a single polynomial function. In order to achieve a reasonable fit, the data are fit in two segments, with one function covering the MLST range -2 to 8 hours, and the second covering hours 6.5 to 26. The two fits agree well at a MLST values of 0 and 7.5 hours so these are used as the transition points between the two functions.

Figure 30 shows the data values as individual black dots. The green line traces the binned values and the red line shows the model fit. There is a horizontal line drawn between the model values at 0 and 24 hours to show that the values are nearly, but not exactly equal. There is also a vertical line drawn at MLST = 7.5 hours to show that the morning transition between the polynomial functions is smooth. The fit coefficients are given, along with the chi-squared values of the two fits. The IFG sensor temperature profile has been fairly stable since landing and there has been no need to update the fit parameters using data acquired in 2019. The data are routinely checked against the model and the model will be updated in the future if required.

Figure 30: Polynomial fit to the IFG sensor temperature data.

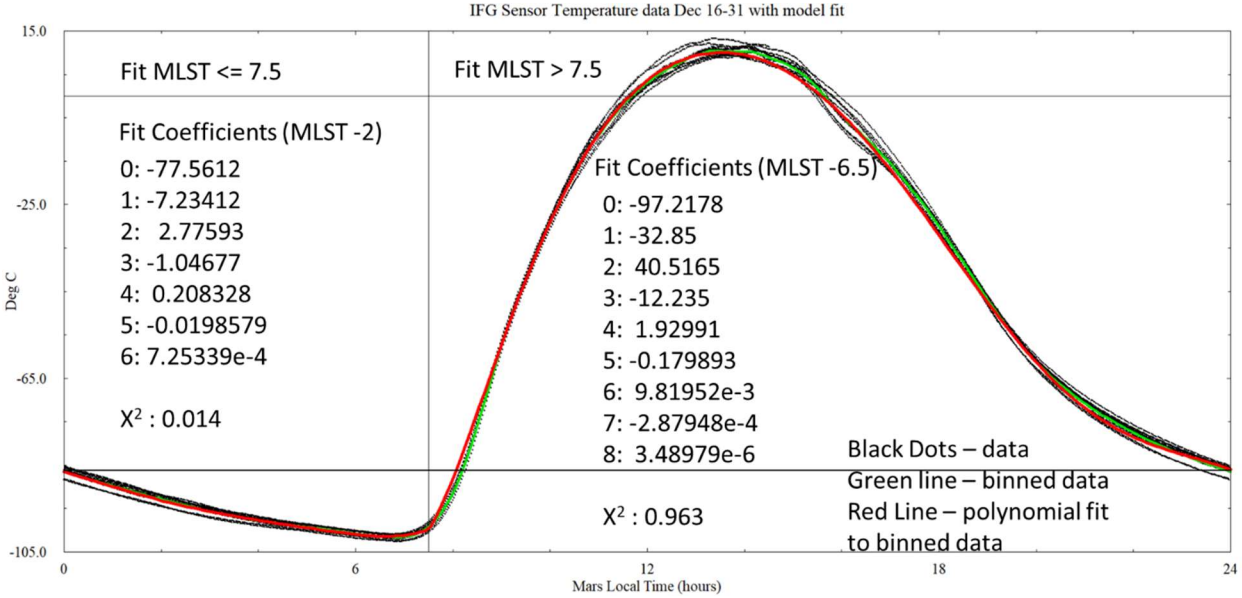

The DQF value in the calibrated data set is used to identify the source of the sensor temperature data used in the calibration process. The 2^2 place is where this information is stored and the value

is set to 0 if actual data are used and is set to 3 for samples where the model temperature was used.

Appendix 2: IFG Electronics Temperature

The IFG calibration is also a function of the electronics temperature. Unfortunately, only temperature a few samples are returned to the spacecraft ground per data processing session so the actual data can't be used for either the data processing or even to develop a model like has been done for the sensor temperature data. Fortunately, there is a temperature measurement for the PAE electronics box in the spacecraft engineering and ancillary data (T-0014) which serves as a reasonably good proxy for the missing data. Unfortunately, this channel is not sampled and returned continuously each Mars day. In general, the channel is frequently sampled when the solar arrays are generating power and is infrequently sampled when the spacecraft is running on its batteries. Since the value is needed continuously for the IFG data processing, these data also need to be fit with a continuous function. The electronics temperature profile is much more variable from day to day than the IFG sensor temperature profile so it is not a good candidate for modeling. Instead, the data points from each week are fit to a continuous function, a running polynomial fit is computes and this fit value (modelET) is stored and used in the data processing.

Figure 31: IFG Electronics temperature data and fits.

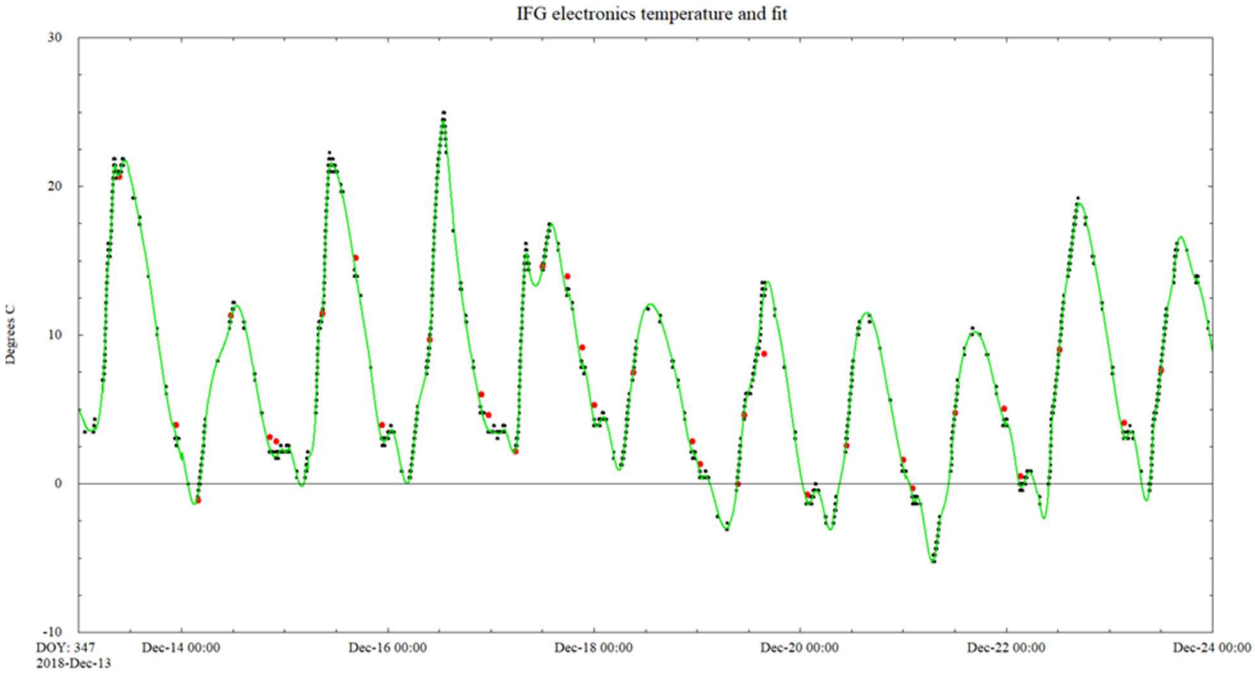

Figure 31 shows the few IFG electronics temperature samples as large red dots, the PAE box temperature (T-0014) values as smaller black dots, and the running fit to the PAE temperature values as the green trace for 11 days in December 2018. The green trace fits the black dots well when the temperature is varying smoothly but it smooths out high frequency fluctuations. The red dots lie along the green trace when the temperature is rising steadily for hours. However, when the temperature is cooling, the actual electronics temperature values are generally displaced to the

right of the green trace indicating that the IFG board is cooling more slowing than the electronics box where it is housed. Note that Figures 5 and 6 in the ground calibration section demonstrate that a few degrees of error in the electronics temperature estimate would only produce a small fraction of a nanoTesla error in the calibrated field for a field of 1000 to 2000 nT. The 2^3 place in the DQF value is always set to a value of 2 to indicate that the electronics temperature is approximated by a fit to the data.

Appendix 3: Fixed Solar Array Currents

The IFG data were shown to be correlated with the fixed solar array current values reported in SCEA channels E-0771 and E-0791. Unfortunately, like the PAE temperature data, these parameters are not returned continuously so the actual data values can't easily be used in the data processing pipeline. The shape of the fix solar array current versus MLST function has been found to be fairly stable in the time since the spacecraft landed so this parameter lends itself to modeling rather than fitting. There were shape and amplitude variations with time that occurred throughout the mission so the shape models used by the data processing pipeline evolve with time.

Figure 32: Fixed solar array current shape model, Dec 14-31, 2018.

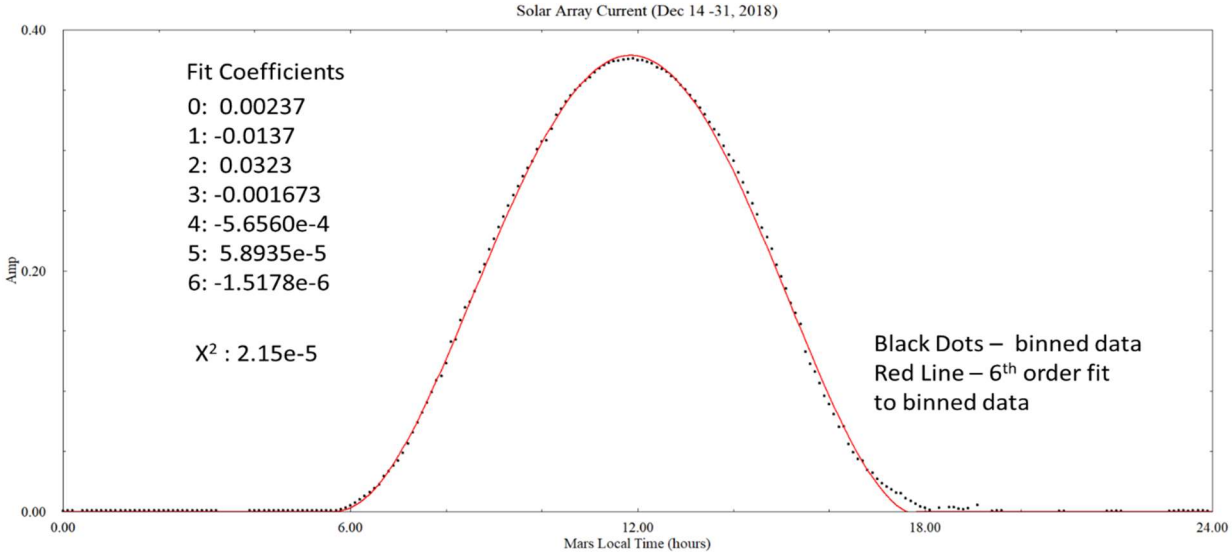

Figure 32 shows a 6th order polynomial fit to the data in channel E-0771 for the time period between December 14 and 31, 2018. The data were binned (black dots) and fit (red trace). The fit coefficients and chi-square value are given in the figure. Figure 33 shows the data (black dots) and model fit (red trace) for the time period in mid-January 2019, when the models were changing in amplitude.

Figure 33: Fixed solar array current and models, January 2019.

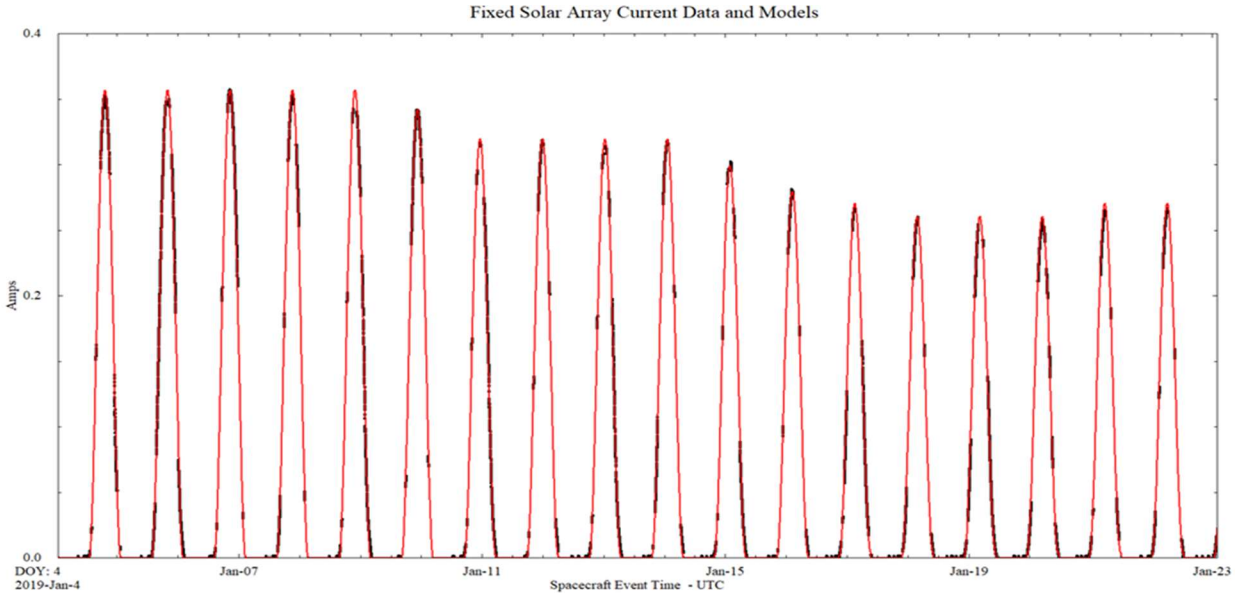

The 2^4 place in the DQF value is always set to a value of 2 to indicate that the fixed solar array current correction is computed using a model fit to the data.

Appendix 4: Total Solar Array Current

The term total solar array current is slightly misleading because the value actually computed and modeled (modSACT) is the total solar array current minus the fixed solar array current, which is a mouthful. Since the fixed solar array currents are modeled separately, it's the remained current that needs to be characterized. When the terms total solar array current or total current are used here, please understand that this is just a shortened way of describing what is a being computed which is the sum of the SCEA channels E-0772 and E-0792. Like the PAE box temperature, the total current data are not returned continuously, nor are the values sampled frequently enough to use them directly in the data processing pipeline.

Figure 34 shows total solar array currents for two days in March 2019 when the data were more continuous than they are normally. In each panel, the top trace is the MLST value and the bottom trace shows the total current data points. Both panels are marked with vertical lines at various values of MLST. The top panel (A) shows data from March 20 and the bottom panel (B) shows March 22, 2019. In both panels, currents start being measure a little before 5.5 hours MLST (first vertical line) and they begin to rise smoothly shortly thereafter. Both panels show the current reaching a maximum value near 10.5 hours MLST, although there is some variation between the two days. On the right side of the figure, both panels show a smooth decay of the current beginning at about 16.4 hours MLST and the current is near zero by 18.5 hours. However, the behavior of the current between about 10.5 and 16.4 hours MLST varies significantly between the two days. Both days show a lot of noise in the data in this time period and both show a rapid

Figure 34: Total Solar Array Current on two days in March, 2019.

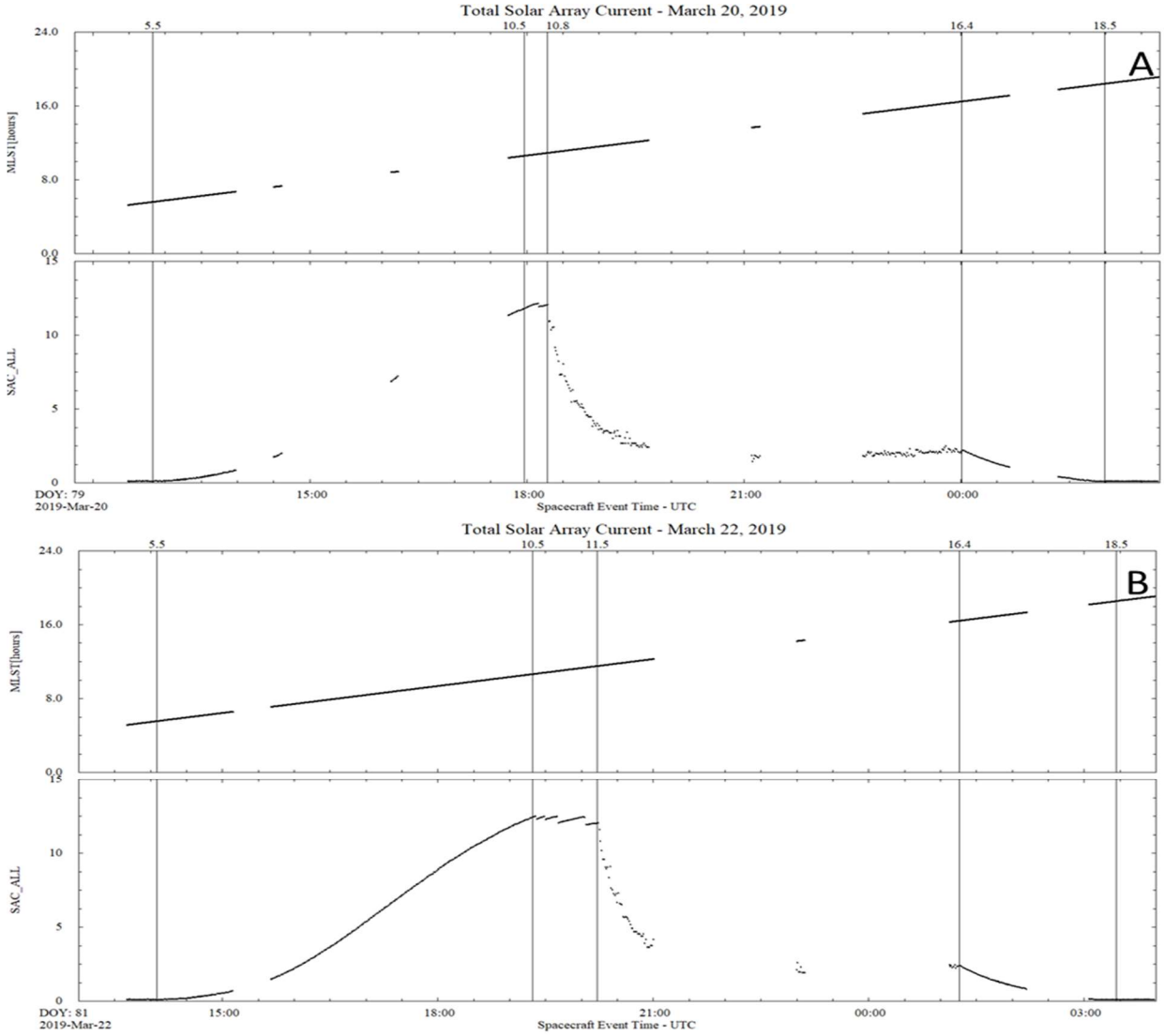

drop to an intermediate current level before decaying to zero at the end of the day. This behavior is normal for this parameter. There is a smooth rise in the early to mid-morning and an evening fall off that are consistent from day to day. However, the mid-day behavior differs in the details and timing but always shows a rapid decline to an intermediate level that is maintained until the evening. In order to model this behavior, the Mars day is split into 4 segments, morning (5.5-10.5), mid-day (11-16.4), evening (16.4 – 18.5), and night (18.5 to 5.5) hours MLST. The night time values are set near zero, the morning and evening values are binned and fit to functions of MLST that are fixed, and the mid-day period is binned and set to another function that is allowed to shift in MLST by as much as ± 0.7 hours MLST. Morning and evening models take precedence over the mid-day model and gaps in MLST coverage are spanned by linearly interpolating between functions. The timing and slope of the morning rise and evening fall-off changes occasionally so data need to be monitored regularly to see if a new base model needs to be computed.

Figure 35:Model of the total solar array current.

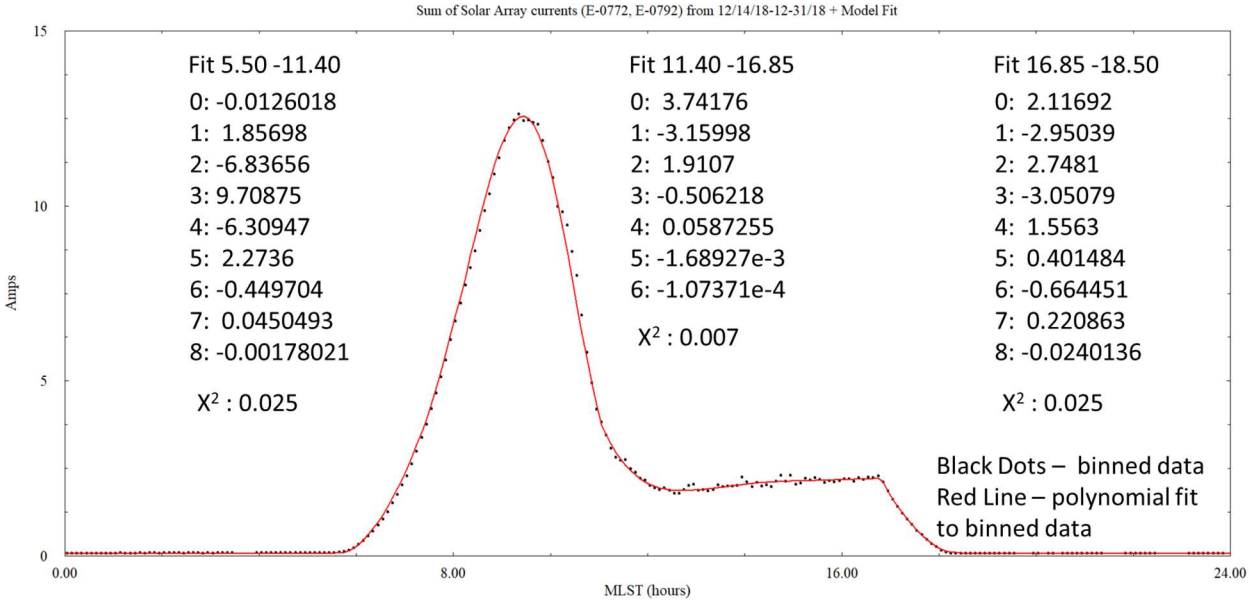

Figure 36: Total solar array current data and model

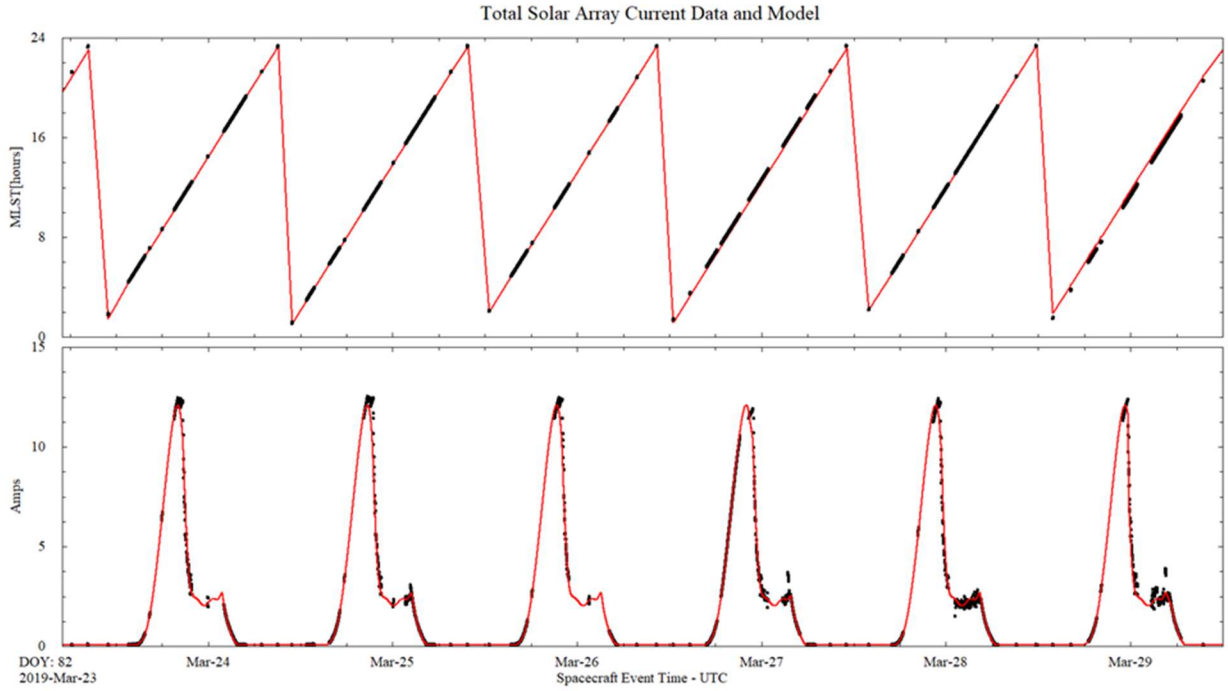

Figure 35 shows total current binned data (black dots) from Dec 14 to 31, 2018 and the morning, mid-day, and evening polynomial fits to the data. Note that mid-day and evening segments begin later in this time period that is does in March 2016. Any time that the shape or amplitude of the models changed, a new model was generated. Models typically remained valid for a few days to a week. Some smoothing is applied to the model dBs to prevent jumps in the data at the shape model boundaries.

Figure 36 shows a bit more than five days of solar array current data (black dots, bottom panel) as well as the model current used to correct the IFG data (bottom panel, red trace). The top panel shows the actual MLST values as black dots and the red trace shows the shifted values used for computing the mid-day model segments. When the mid-day segment has been shifted relative to the morning and evening segments, the missing MLST coverage is computed by linearly interpolating across the gap.

Finally, the 2^5 place in the DQF value is always set to a value of 3 to indicate that the total solar array current correction is computed using a model fit to the data.